Hdb Env Chem Vol. 2, Part N (2006): 209–249
DOI 10.1007/698_2_007

Published online: 20 October 2005

Controls on the Carbon Isotopic Compositions of Lipids in Marine Environments

Richard D. Pancost[1] (✉) · Mark Pagani[2]

[1]Organic Geochemistry Unit, Biogeochemistry Research Centre, School of Chemistry, University of Bristol, Cantock's Close, Bristol BS8 1TS, UK
R.D.Pancost@bristol.ac.uk

[2]Department of Geology and Geophysics, Yale University, PO Box 208109, New Haven, CT 06520, USA

Abstract Organic carbon isotopes have long been used to study modern and ancient biogeochemical processes. Controls on the isotopic composition of organic matter in marine sediments range from the sources of the organic matter (e.g. allochthonous vs. autochthonous inputs) to the physiology of the predominant photoautotrophs, the nutrient status of the photoautotrophs' growth environment and the degree of organic matter reworking by heterotrophic eukaryotes and bacteria. The diversity and antagonistic effects of these variables make it difficult to interpret the bulk organic carbon isotope record; consequently, the use of gas chromatography–combustion–isotope ratio monitoring mass spectrometry (GC–IRMS) to determine the carbon isotopic compositions of specific compounds (compound-specific carbon isotope analysis; CSIA) has become a widely used tool in palaeoclimate and ecological investigations. Here, we summarize the main controls on the $\delta^{13}C$ values of lipids found in marine environments and illustrate their utility with several case studies.

1 Introduction

The organic matter occurring in modern or ancient settings represents an archive of potential insight into the organisms and environmental conditions of those settings. Commonly, this information is extracted via the chemical composition of the organic matter—with potentially useful compounds ranging from diagenetically and catagenetically altered lipids that can be traced to specific biological precursors (biomarkers) to pigment distributions that can be used to reconstruct modern phytoplankton assemblages. In addition to the chemical structure of organic matter, much additional information is preserved in the isotopic composition of that organic matter. In particular, the carbon isotopic composition of marine organic matter has commonly been used in a variety of ecological and palaeobiological investigations. These initial investigations utilized the fact that organic matter produced by organisms employing the Calvin cycle (also referred to as the Calvin–Benson cycle) is characteristically depleted in ^{13}C relative to inorganic carbon substrates. Hence, Schidlowski [1] invoked the ^{13}C-depleted character of ancient organic matter as evidence for photosynthesis on the ancient earth, while others recognized it as further evidence for the biological origin of petroleums. Scientists also realized that a variety of processes, including diagenesis [2], catagenesis [3] and heterotrophic reworking of organic matter [4–6], imposed secondary controls on its carbon isotopic composition. This latter observation, combined with analogous observations for organic matter $\delta^{15}N$ values, served as the basis for trophic studies of marine food webs [4].

More recently, recognizing that photoautotrophs have widely varying carbon isotopic compositions, scientists have attempted to constrain the controls on carbon isotope fractionation during photosynthesis; this has served as the basis for additional applications in palaeoenvironmental research.

Calder and Parker [7], Morris [8] and Degens et al. [9] all observed that microalgae grown in cultures became more depleted in ^{13}C as the amount of supplied CO_2 increased. These observations led workers to interpret anomalously light carbon isotopic values in geological samples as indicators of high pCO_2 [10, 11]. Subsequent developments have refined the approach of these early workers, but the principles remain the same and organic matter $\delta^{13}C$ values remain a widely used palaeo-pCO_2 proxy [12], although further work indicates that other variables also govern algal $\delta^{13}C$ values and must be considered.

While the diversity of controls on organic matter $\delta^{13}C$ values presents the opportunity for their application to diverse investigations, they also make it difficult to interpret the bulk organic carbon isotope record. Consequently, the use of gas chromatography–combustion–isotope ratio monitoring mass spectrometry (GC–IRMS) to determine the carbon isotopic compositions of specific compounds (compound-specific carbon isotope analysis; CSIA) has become widespread. By using this approach, primary versus secondary and allochthonous versus autochthonous organic materials can be isotopically distinguished, and pCO_2 reconstruction can be based on compounds derived from a narrow range of organisms rather than the physiologically diverse sources of organic matter present in most marine settings. Moreover, the information recovered from a single sample is much more diverse: insight into algal photosynthesis, higher plant community structure on adjacent land masses and bacterial recycling of organic matter can be elucidated from a few analyses [13]. However, this approach also introduces additional complications related to carbon isotope fractionation during the synthesis of specific compound classes [14, 15]. Here, we discuss the main controls on the $\delta^{13}C$ values of lipids found in marine environments and illustrate their utility with two case studies.

1.1 Background

The relative abundances of stable isotopes are usually expressed as ratios, with the lighter isotope in the denominator, e.g. $^{13}C/^{12}C$ ($^{h}X/^{l}X$). Because variations in isotope ratios are small and measured against standards of known isotopic composition, the isotopic compositions of natural materials are reported as $\delta^{h}X$ values (parts per mil ‰).

$$\delta X(\%) = \left(\frac{R_{\text{sample}} - R_{\text{standard}}}{R_{\text{standard}}} \right) \times 10^{3} \quad \text{where } R = {}^{h}X/{}^{l}X \tag{1}$$

Thus, a $\delta^{h}X$ value of 0‰ indicates that the isotopic composition of the sample is identical to that of the standard, positive $\delta^{h}X$ values indicate that the sample is enriched in the heavy isotope relative to the standard, and negative $\delta^{h}X$ values indicate that the sample is depleted in the heavy isotope relative to the

standard. Carbon isotopic compositions are expressed relative to the primary standard Vienna Pee Dee Belemnite (VPDB) as described above:

$$\delta^{13}C = ({}^{13}R_{SA}/{}^{13}R_{VPDB} - 1) \times 10^3 \quad (2)$$

where ${}^{13}R_{SA}$ and ${}^{13}R_{VPDB}$ represent the ${}^{13}C/{}^{12}C$ abundance ratios for the sample and VPDB, respectively.

Variations in relative isotopic abundance are a consequence of the preferential reaction of one isotopic species over another. This arises as a direct result of differences in the energies of molecules comprised of different isotopes of the same element, with molecules containing the light isotope generally existing at a higher energy level. This means, for example, that a bond between the light isotope and another atom will break more rapidly than a comparable bond involving the heavy isotope. This leads to isotopic fractionation, without which natural isotopic variation would not exist. Fractionation can occur during a variety of physiochemical processes, for example chemical reactions, phase changes and molecular diffusion, but is always defined as:

$$\alpha = \frac{R_{products}}{R_{reactants}} \quad (3)$$

The fractionation factor represents the degree of depletion in the instantaneous product of a reaction. In a closed system, characterized by a normal isotope effect (where the light isotope reacts more quickly), the accumulated product (initially the instantaneous product) gradually becomes less depleted in the heavy isotope. When the reaction goes to completion, the isotopic composition of the product is the same as that of the initial reactant, i.e. no enrichment or depletion of the product is observed. This is known as Rayleigh fractionation and is represented by:

$$\frac{R}{R_0} = f^{(\alpha-1)} \quad (4)$$

where R_0 is the isotopic ratio of the reactant at time zero and f is the fraction of the reactant remaining.

Changes in isotopic composition associated with a reaction are also commonly reported as isotope effects or enrichment factors (ε) [16]; if the fractionation factor differs from 1 by less than 5%, then:

$$\varepsilon = (\alpha - 1) \times 1000 \quad (5)$$

The latter relationship is similar to the commonly used isotope discrimination term Δ:

$$\Delta = (\alpha - 1) \times 1000 \sim \delta_{products} - \delta_{reactants} \quad (6)$$

Again, this relationship is only valid if $\alpha \sim 1$.

1.2 Isotope Analysis

All mass spectrometers can measure isotope ratios, but in practice only Nier-type isotope ratio mass spectrometers (IRMS) have sufficient precision to measure variations at natural abundances (4–6 significant figures). These mass spectrometers are fitted with double or triple ion collectors, and traditionally use dual-inlet systems allowing rapid switching between standard and samples. One of the most important advances in analytical chemistry in the past 20 years has been the development and widespread application of continuous-flow isotope ratio mass spectrometry (CF-IRMS) [17–19]. Continuous-flow mass spectrometers can operate at the higher pressures associated with the continual influx of helium, allowing online introduction of small quantities of analyte. Consequently, CF-IRMS allows the isotopic composition of chemically diverse materials to be determined much more rapidly and at significantly lower quantitites (< 100 ng of the element of interest) than traditional offline approaches. Moreover, the development of sophisticated interfaces for IRMS now allows the isotopic characterization of diverse organic and inorganic materials. Coupling of a gas chromatograph (GC) to the IRMS via a combustion interface, which converts eluting compounds into CO_2 and H_2O, enables carbon isotopic compositions to be determined for specific compounds in complex mixtures [5].

Determination of compound-specific $\delta^{13}C$ values is obviously contingent not only on the mass spectrometer but also on the analytical work-up prior to analysis and the resolvability of compounds by gas chromatography. The methods traditionally used in the organic geochemistry field are well established, involving a combination of extraction, compound class fractionation and chemical degradation approaches, and have been discussed in detail elsewhere. Upon appropriate derivatization of polar compounds (e.g. methylation of carboxylic acids, conversion of alcohols into their corresponding trimethylsilyl ethers), compound fractions can be analysed by GC–IRMS. Although specific approaches vary depending on the analyte and instrument used, the general operating principles are the same for all GC–IRMS systems. Sample aliquots are injected into the GC and the compounds are partitioned on a capillary column as in normal GC or GC–MS operation; however, eluting compounds are passed through an oxidizing furnace, which converts organic compounds into CO_2 and H_2O. The H_2O is subsequently removed and CO_2 enters the mass spectrometer through a continuous-flow interface.

2
Common Prokaryotic and Eukaryotic Biomarkers in Marine Sediments

The utility of compound-specific isotope analysis is directly related to the specificity of the compounds being analysed. Compounds with very specific sources, such as alkenones derived from certain species of haptophyte algae, provide more precise data, allowing the most constrained interpretation, but less diagnostic compounds can still provide useful information in the proper context. It is not the role of this chapter to provide a complete discussion of compounds typically examined during isotopic investigations nor the caveats associated with their source assignments; however, it is useful to describe some of the most commonly analysed compound classes.

2.1
Algal Lipids

The lipids of marine and lacustrine algae, their degradation pathways and representative biomarkers in the geologic record have been studied for decades [20–23], and this literature is only briefly summarized here, with particular emphasis on compounds used in carbon isotope studies. Alkenones, long-chain ($C_{37} - C_{39}$) unsaturated ethyl and methyl ketones produced by only a few species of Haptophyte algae in the modern ocean [24–26], are the most commonly used algal biomarkers in environmental investigations due to their relative ease of preparation and isotopic analysis, source specificity, diagenetic robustness and the use of their distributions as a sea surface temperature proxy [26, 27]. Controls on their carbon isotopic composition and application to environmental studies are described in Sect. 7.1. After alkenones, steroids are the algal lipids most commonly investigated using isotopic approaches. Because of their structural diversity [22, 28], certain sterols are relatively diagnostic for specific taxa. For example, 24-methylcholesta-5,22*E*-dien-3β-ol and especially 24-methylcholesta-5,24(28)-dien-3β-ol have both been invoked as diatom biomarkers, although these sterols are also present in other algae [28]. More diagnostic are the 4-methylsterols, especially 4α,23,24-trimethyl-5α-cholest-22*E*-en-3β-ol (dinosterol), as biomarkers for dinoflagellates [29–31]. Several workers have determined sterol $\delta^{13}C$ values in modern surface waters [32–35] and shallow marine sediments. Sterol $\delta^{13}C$ values have been used to either clarify the sterol sources (e.g. that 24-ethylcholesterols in Peru surface waters derive from diatoms and not higher plants [33]), or evaluate controls on algal growth rates. In ancient sediments, steranes are among the most abundant preserved hydrocarbons; however, thermal isomerization typically results in a complex distribution of steranes and determination of the $\delta^{13}C$ values of specific compounds is difficult [36].

Other diagnostic compounds that could serve as useful algal biomarkers in isotopic studies are C_{20}, C_{25} and C_{30} highly branched isoprenoids (derived

from diatoms [37, 38]), long-chain alkyl diols (derived from eustigmatophytes and other microalgae [28, 39]) and highly unsaturated fatty acids [40, 41]. However, isotopic studies of such compounds are relatively uncommon and future research on cultured organisms and modern marine environments is critical.

Chlorophylls and their degradation products, while not as diagnostic as the aforementioned compounds, can be used as tracers for the isotopic composition of the entire algal community. Because they are not amenable to GC, it is difficult to directly determine chlorophyll (and porphyrin) $\delta^{13}C$ values, and most efforts have focussed on their degradation products. Phytol, the esterified side chain of most chlorophylls, and inferred hydrocarbon degradation products (pristane, phytane) have been the subject of compound-specific carbon isotopic analysis since the advent of the technique [5, 13]. However, sedimentary pristane and phytane can have higher plant sources [42] and some workers have focussed on examining S-bound phytane as a more specific photoautotroph biomarker [43]. Maleimides, 1-*H*-pyrrole-2,5-diones, are direct degradation products of the chlorophyll and bacteriochlorophyll tetrapyrrole structure, are common in extracts of ancient sediments and are amenable to GC [44]. Thus, maleimide $\delta^{13}C$ values are relatively easy to determine and have been used to gain insight into carbon cycling in ancient settings (e.g. Permian Kupferschiefer [44]).

2.2 Lipids from Higher Plants

Long-chain *n*-alkyl compounds are major components of epicuticular waxes from the leaves of vascular plants [45]. These compounds are relatively resistant to degradation, which makes them suitable for use as higher plant biomarkers [46], and include *n*-alkanes, *n*-alkanols, *n*-alkanoic acids and wax esters. *n*-Alkanes occur in vascular plant leaf extracts with carbon chain-lengths ranging from C_{25} to C_{35} [45, 47] and with a strong predominance of odd-carbon-number homologues over even-numbered ones. The *n*-alkanols and *n*-alkanoic acids typically occur in higher plants as the $C_{26} - C_{34}$ homologues with a strong even-over-odd predominance, reflecting their biosynthesis from acetyl moieties [47, 48]. It is relatively easy to determine carbon isotopic compositions of higher plant *n*-alkyl compounds using GC–IRMS, because they commonly occur in high abundances and relatively simple adduction procedures can be used to obtain pure fractions. Thus, the carbon isotopic compositions of these compounds in modern plants, soils and lacustrine and marine sediments have been extensively published. A variety of pentacyclic triterpenoids, typically with structures based on the ursene, oleanene or lupene hydrocarbon skeletons, are common in higher plants. Due to their ubiquity, such compounds are typically only used as general tracers of higher plant input. However, oleanoids and lupanoids, deriving only from angiosperms, and taraxeroids, thought to derive predominantly from

mangrove leaves [49], can be more specific higher plant tracers. Although triterpenoids are often abundant in marine and terrestrial sediments, their $\delta^{13}C$ values have been rarely published. This is mainly due to co-elution with other compounds, including steroids and bacterial hopanoids.

Higher plant macromolecular components in sediments include resin- and lignin-derived compounds. Lignin, a relatively stable and microbially resistant heteropolymeric structure comprised of phenylpropanoid subunits [50], is a significant component of wood and occurs in the cell walls of all vascular plant tissue. Moreover, lignin monomers have different sources [51, 52] and the isotopic compositions of syringyl, vanillyl and cinnamyl phenols can be used to distinguish isotopic signals of different plant types [53, 54]. Although preparation of lignin monomers for isotopic analysis requires careful chemical work-up, typically involving CuO oxidation of the lignin macromolecule, generated fractions are readily analysable by GC–IRMS.

2.3 Bacterial and Archaeal Lipids

The most common bacterial biomarkers in marine sediments are free and bound (phospholipid) fatty acids, of which the latter comprise the membranes of bacteria; however, eukaryotes also contain membranes comprised of phospholipid fatty acids and these compounds are not diagnostic as a class. The most common, such as saturated C_{16} and C_{18} fatty acids, are particularly widespread and appear to have little utility as tracers of explicit prokaryotic processes. However, some fatty acids, characterized by site-specific methyl groups, double bonds or cyclic moieties, are less common. Other bacterial membrane lipids are the hopanoids, pentacyclic triterpenoids common in cyanobacteria, methanotrophs and aerobic heterotrophic bacteria [55–57]. Until recently, hopanoid structures had not been found in cultures of anaerobic bacteria and were thought to be largely diagnostic for aerobic organisms [55]. However, the occurrence of ^{13}C-depleted hopanoids in Black Sea sediments is evidence for at least one anaerobic source [58]. Moreover, hopanoids have recently been recovered in anaerobic cultures containing predominantly anaerobic ammonia-oxidizing bacteria (Annamox) [59]. The most commonly observed hopanoids are diplopterol and bacteriohopanpolyol derivatives. During diagenesis, vicinal cleavage of the bacteriohopanpolyol side chain results in the formation of, typically, bishomohopanol and eventually bishomohopanoic acid. Both of these compounds are typically well resolved during GC analysis of marine sediments and their $\delta^{13}C$ values can be readily determined. In contrast to the widely occurring hopanoids, the methylhopanoids appear to be more source-diagnostic, with 3β-methylbacteriohopanoids being relatively specific for some methanotrophs [60] and 2β-methylbacteriohopanoids being common in and largely restricted to cyanobacteria [57]. However, due to co-elution with the more abundant hopanoids, precise determination of methylhopanoid $\delta^{13}C$ values is difficult.

In addition to the above widespread bacterial biomarkers, a variety of compounds are biomarkers for photosynthetic bacteria. These include biomarkers for cyanobacteria, including monomethyl alkanes [61, 62], and diverse pigments, including isorenieratene [63], chlorobactene and bacteriochlorophylls *d* and *e*, which are diagnostic for green sulphur bacteria. Of these, it is relatively easy to determine $\delta^{13}C$ values for isorenieratene derivatives (especially isorenieratane) due to their high molecular weight and long retention time eliminating most co-elution problems. Even in samples where co-elution does occur, clean fractions can be readily obtained by thin-layer chromatography [64].

Archaeal membrane lipids are distinct from those of the bacteria and eukarya because they contain isoprenoidal alkyl units ether-bound to a glycerol backbone rather than ester-linked alkyl components [65]. Archaeol is the most common of the archaeal diethers [66], while hydroxyarchaeol has the same core structure as archaeol but contains an additional hydroxyl group on the third carbon of the phytanyl moiety ether-linked to either the third (*sn*-3-hydroxyarchaeol) or second (*sn*-2-hydroxyarchaeol) glycerol carbon. Like diethers, glycerol tetraethers (glycerol dialkyl glycerol tetraether; GDGT) are diagnostic for, and common in, archaea. In archaeal tetraethers, the alkyl groups are biphytane units with zero to four cyclopentane rings. The GDGT composed of two acyclic biphytanyl units is apparently widespread in archaea [67], whilst GDGTs containing biphytanyls with cyclopentane units were previously thought to be present only in thermophilic archaea [65]. However, recent work has revealed that GDGTs containing biphytanyl groups bearing one or two cyclopentane rings occur in mesophilic settings [66–72]. In general, archaeol and hydroxyarchaeol elute during gas chromatography after other common biomarkers such as steroids and alkenones, such that it is relatively straightforward to determine their $\delta^{13}C$ values in samples where they are abundant. In contrast, GDGTs are not amenable to GC using standard approaches and determination of their $\delta^{13}C$ values requires chemical degradation, typically with HI acid followed by $LiAlH_4$ reduction, to release biphytanes [66]. Other archaeal biomarkers include the irregular isoprenoids 2,6,10,15,19-pentamethylicosane (PMI) and crocetane and their unsaturated derivatives; these compounds have only been identified in association with methane cycling and appear to derive from either methanogens or anaerobic methane-oxidizing archaea [73–78].

3 Controls on Algal $\delta^{13}C$ Values

Although biomass and lipid $\delta^{13}C$ values can differ significantly among phytoplankton, bacteria, archaea and higher plants, the underlying controls on the carbon isotopic compositions in all organisms are intrinsically the same and

depend on the isotopic composition of the carbon source and the mechanisms by which that carbon is assimilated.

3.1 The Carbon Isotopic Composition of Dissolved Inorganic Carbon (DIC)

Marine photoautotrophs utilize various forms of dissolved inorganic carbon that derive from interactions of seawater with carbon dioxide. The solubility of gaseous carbon dioxide in seawater, and its subsequent reaction with H_2O, results in several dissolved forms of inorganic carbon including aqueous carbon dioxide (CO_{2aq}), carbonic acid (H_2CO_3), bicarbonate (HCO_3^-) and carbonate ion (CO_3^{2-}). The hydration of CO_{2aq} produces H_2CO_3, whereas HCO_3^- and CO_3^{2-} result from the dissociation of H_2CO_3. However, due to the low concentration of H_2CO_3 relative to CO_{2aq} (the other neutral carbon species), and the fact that H_2CO_3 and CO_{2aq} are chemically inseparable, it is conventional to treat the concentrations of H_2CO_3 and CO_{2aq} as singular (i.e. $[CO_{2aq}]$). At equilibrium, the activity of all dissolved carbon species (or less precisely, the concentration of the carbon species), can be determined from Henry's law, and application of the first and second dissociation constants of carbonic acid (Fig. 1):

$$[CO_{2aq}] = [pCO_2]K_H \tag{7}$$

$$[HCO_3^-] = K_1^*[CO_{2aq}]/[H^+] \tag{8}$$

$$[CO_3^{2-}] = K_2^*[HCO_3^-]/[H^+] \tag{9}$$

where K_H is the temperature-, salinity-, and pressure-dependent equilibrium constant of CO_2 solubility [79], and K_1^*, K_2^* are the first and second apparent dissociation constants of carbonic acid.

Associated with the chemical equilibria of the carbonate system are temperature-dependent isotopic fractionations of carbon and oxygen atoms that lead to distinct isotopic compositions for each carbonate species. Carbon isotopic fractionations of the carbonate system maintain quantifiable relationships between aqueous species, with CO_{2aq} depleted in ^{13}C and CO_3^{2-} and HCO_3^- enriched in ^{13}C relative to gaseous CO_2 (CO_{2g}). For example, the isotopic composition of HCO_3^- is $\sim$ 10 and 9‰ greater than that of CO_{2aq} at 15 and 25 °C, respectively. The results of Mook et al. [80] are represented in Fig. 2 as the equilibrium fractionation of each carbon species relative to bicarbonate. Also displayed are the conclusions of Romanek et al. [81], which indicate that calcite and aragonite precipitated in equilibrium are enriched in ^{13}C relative to HCO_3^- by $\sim 1.0 \pm 0.2$ and 2.7 ± 0.6‰, respectively. Furthermore, carbon isotopic fractionations associated with carbonate precipitation are insensitive to temperature between 10–40 °C. In general, recent experimental determinations of carbon fractionations for the carbonate system are in broad agreement. One notable exception is provided by the work of Mook

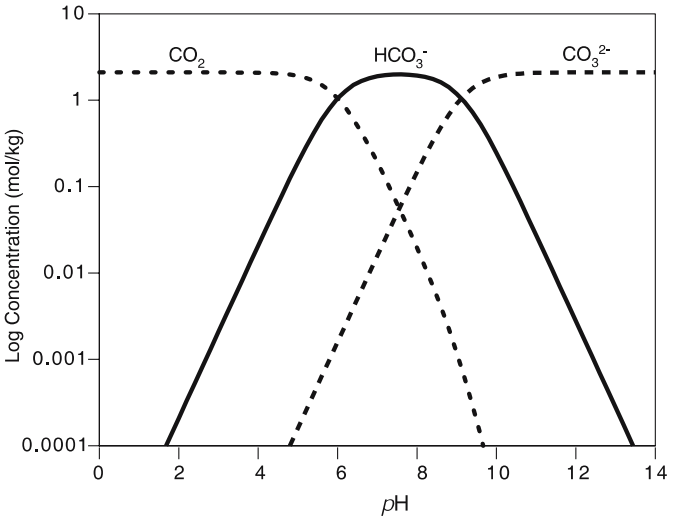

Fig. 1 Concentrations of the dissolved carbon species as a function of pH. $T = 25\,^{\circ}C$, $S = 35$, $\sum CO_2 = 2.1$ mmol

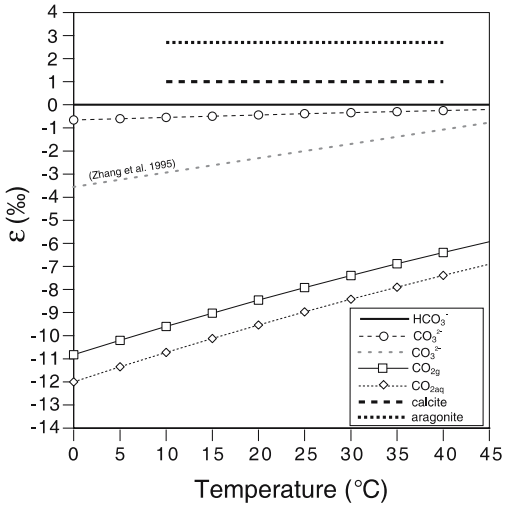

Fig. 2 Carbon isotope fractionations between carbon species of the carbonate system relative to HCO_3^-. Fractionations between dissolved species are from the results of Mook et al. [80] and Zhang et al. [82]. Fractionations between solid phases are from the results of Romanek et al. [81]

et al. [80] and Zhang et al. [82] for the $CO_3^{2-} - HCO_3^-$ equilibrium, which present values differing by $\sim 2.5‰$ at $0\,^{\circ}C$ (Fig. 2). The true nature of the carbon isotopic fractionation that occurs between CO_3^{2-} and other aque-

ous carbon species remains unresolved. However, the recent conclusions of Zhang et al. [82], which predict a larger fractionation for CO_3^{2-} – HCO_3^- relative to that found by Mook et al. [80], are supported by the experimental results of Halas et al. [83] and recent theoretical calculations [84]. A more detailed description of the topic can be found in the article by Zeebe and Wolf-Gladrow [84].

All of these variables must be considered when examining the isotopic composition of ancient organic matter. Past changes in the isotopic composition of the entire ocean–atmosphere reservoir of carbon dioxide are significant [85] and arise from changes in the relative magnitudes of carbon sources (e.g. volcanism, metamorphism, methane clathrate dissolution) and sinks (organic carbon and carbonate burial). Thus, during times of high organic burial, such as the Mesozoic oceanic anoxic events, DIC $\delta^{13}C$ values were about 2 to 3‰ greater [86], while during inferred clathrate release events, ocean DIC $\delta^{13}C$ values were as much as 4‰ lower [87]. Past pH variations in open ocean settings probably exert only a secondary control on substrate and algal $\delta^{13}C$ values (although its influence on carbon availability as discussed below is important), but pH does need to be considered when interpreting isotopic data from alkaline lakes, hydrothermal springs or similar settings.

3.2
Carbon Isotope Fractionation During Carbon Assimilation

Of the dissolved carbon species in seawater, CO_{2aq} and HCO_3^- are the primary forms available for marine algae during photosynthesis. However, the precise pathway of inorganic carbon uptake and utilization for various marine algae is actively debated in the literature. In general, two models for marine carbon fixation are probable: (1) a passive model requiring diffusive transport of CO_{2aq} across the cell membrane, and (2) an active process where HCO_3^- and/or CO_{2aq} is enzymatically transported across the cell membrane or, alternatively, the concentration of extracellular CO_{2aq} is enzymatically amplified to accommodate low ambient [CO_{2aq}]. Both diffusive and carbon-concentrating models predict a large carbon isotope fractionation during photosynthesis due to the influence of ribulose-1,5-bisphosphate carboxylase/oxygenase (rubisco) during carbon fixation via the Calvin cycle. Rubisco displays a fractionation of ca. 29‰ with respect to aqueous CO_{2aq} during in vitro experiments [88, 89]. However, this maximum value is rarely expressed in marine photoautotrophs from natural settings. Smaller in situ fractionations have been attributed to differences in growth rate and cell geometry [90, 91], the influence of β-carboxylase PEPC (phosphoenolpyruvate carboxylase) [92] during carboxylation and/or the active transport of inorganic carbon to the site of fixation [89, 93, 94].

3.2.1 Calvin Cycle

The first step of the Calvin cycle involves the reaction of a molecule of CO_2 with ribulose-1,5-bisphosphate to form an unstable six-carbon intermediate molecule that degrades into two molecules of 3-phosphoglycerate (PGA). PGA, the first component synthesized during the carboxylase reaction, is a three-carbon molecule. Hence, the Calvin cycle is also known as the C_3 pathway. Three molecules of CO_2 are necessary to produce six molecules of PGA. Addition of phosphate groups to six molecules of PGA (derived from ATP) to synthesize six molecules of 1,3-biphosphoglycerate, and subsequent reduction of a carboxyl group and hydrolysis of the phosphate group, forms one molecule of glyceraldehyde 3-phosphate. Glyceraldehyde 3-phosphate is the primary molecule transferred from the chloroplast for the synthesis of carbohydrates.

3.2.2 Fractionation in the Absence of Active Uptake

If CO_{2aq} is supplied to the cell by simple diffusion or if diffusion dominates the transfer of CO_{2aq} from the ambient environment to the site of carboxylation, then the magnitude of total carbon isotope discrimination during photosynthesis (ε_p) is a function of the isotope fractionations associated with carbon transport and fixation, and the concentrations of extra- and intercellular CO_{2aq}:

$$\frac{\delta_a - \delta_{org}}{1 + \delta_{org/1000}} = \varepsilon_t + (\varepsilon_f - \varepsilon_t)\frac{C_i}{C_e} \tag{10}$$

where ε_p is equivalent to the left side of Eq. 10, and δ_a and δ_{org} are the carbon isotopic compositions of the substrate inorganic carbon and algal organic carbon, respectively. The terms ε_f and ε_t are carbon fractionations associated with carbon fixation and diffusive transport, and C_e and C_i are extra- and intercellular [CO_{2aq}], respectively. This model derives from, and is equivalent to, the model of C_3 photosynthesis in higher plants [95].

Equation 10 indicates that the intercellular pool of carbon dioxide (C_i) exerts considerable influence on the magnitude of ε_p values for marine algae. However, the concentration of intercellular CO_{2aq} is rarely known. Thus, C_i can be described in terms of C_e and the specific growth rate (μ) of the cell (i.e. the net flux of CO_{2aq} divided by the carbon content per cell), allowing Eq. 10 to be recast [96, 97]:

$$\varepsilon_p = \varepsilon_t + (\varepsilon_f - \varepsilon_t)\left(1 - \frac{\mu C}{kC_e}\right) \tag{11}$$

where C is the carbon content of the cell and k is the rate constant for the diffusion of CO_{2aq} into and out of the cell, which is equivalent to the permeability of the cell membrane to CO_{2aq} [96].

This formulation reasonably assumes that resistance to diffusion of CO_{2aq} into and out of the cell are the same. Furthermore, the permeability of the cell membrane is likely to be proportional to the surface area of the cell [91, 96, 98], whereas the carbon content of the cell is proportional to the cell volume [91, 99].

Equation 11 predicts a linear relationship between ε_p versus the ratio $\mu/[CO_{2aq}]$ with maximum fractionation occurring under high $[CO_{2aq}]$ and/or as μ approaches zero. Support for the model described in Eq. 11 is found in chemostat incubations performed under nitrate-limited conditions for some algae including alkenone-producing haptophyte algae *Emiliania huxleyi* [90], and the diatoms *Phaeodactylum tricornutum* [96] and *Porosira glacialis* [91]. In these three experiments, ε_p varied linearly with respect to $\mu/[CO_{2aq}]$, each with different slopes and identical y-intercepts (Fig. 3a). The y-intercept ($\sim$ 25‰) reflects the value of ε_f as $\mu/[CO_{2aq}]$ approaches zero. A similar value for both coccolithophorids and diatoms suggests that 25‰ is the maximum value of ε_f for marine algae utilizing a combination of rubisco and β-carboxylases [100]. A wider range of values for ε_f ($\sim$ 22.5–26.6‰) is statistically plausible from evaluation of the same data set [12]. However, a value of 25‰ is consistent with calculated estimates

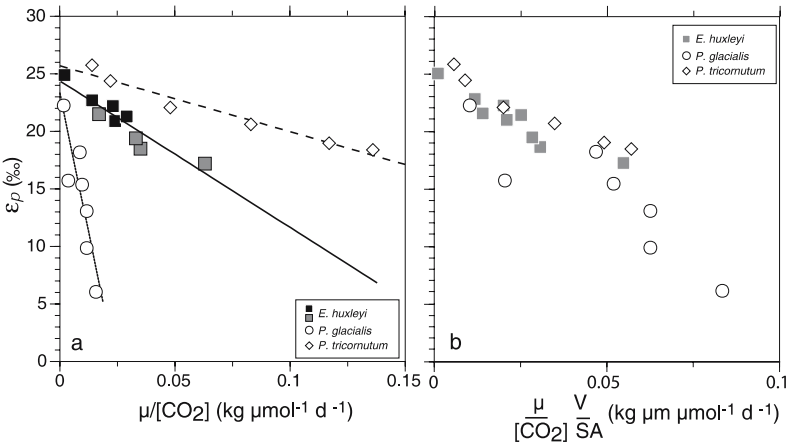

Fig. 3 Comparison of ε_p versus $\mu/[CO_{2aq}]$. **a** Chemostat incubations (from [91]). All experiments were conducted under nitrate-limited, continuous light conditions, except for *P. tricornutum* which includes both continuous light and 12 : 12-hour light/dark cycles. *P. tricornutum*, *open diamonds* (from [211]); *E. huxleyi*, *squares* (calcifying: *filled squares*, noncalcifying: *shaded squares*) (from [90]); *P. glacialis*, *open circles* (from [91]). **b** Comparison of ε_p versus ($\mu/[CO_{2aq}]$) (volume/surface area) (from [91])

of 25–28‰ for algae with C_3-type metabolisms, assuming a 2–10% contribution of β-carboxylation to the total carboxylation [101]. Importantly, differences in slopes for ε_p versus $\mu/[CO_{2aq}]$ can be normalized by accounting for differences in cell geometries, specifically the ratio of volume to surface area (Fig. 3b). This observation supports assumptions regarding the relationships between permeability and cell surface area, carbon content and biovolume [91]. However, a linear relationship for ε_p versus $\mu/[CO_{2aq}]$ can also be explained by models incorporating the effects of active carbon uptake and, thus, is not proof of a diffusive carbon uptake model [91].

3.2.3
The Impact of Active Uptake of Dissolved Inorganic Species on Algal $\delta^{13}C$ Values

Various algae have been shown to have an inducible carbon concentrating mechanism (CCM) when $[CO_{2aq}]$ is lowered such that it becomes limiting to growth [93, 102, 103]. Burns and Beardall [102] demonstrated on the basis of intercellular pH that the marine microalgae *Phaeodactylum tricornutum, Dunaliella tertiolecta, Isochrysis galbana,* and *Porphyridium purpureum* grown in batch cultures under continuous light had the capacity to increase internal $[CO_{2aq}]$ by three to seven times relative to ambient concentrations ($\sim 12\ \mu M$). Further, these authors argue [102] that the presence of extracellular carbonic anhydrase, an enzyme that catalyses the dehydration of HCO_3^-, does not support the active transport of HCO_3^-. More likely, CO_{2aq} is actively or diffusively transported across the plasmalemma, with the potential for active transport of HCO_3^- at the chloroplast envelope.

Sharkey and Berry [93] assessed the carbon source utilized during the growth of *Chlamydomonas reinhardtii* by tracking changes in the $\delta^{13}C$ value of residual air. In these experiments, microalgae grown under high $[CO_2]$ ($3300\ \mu L\ L^{-1}$) were transferred to a medium with low $[CO_2]$ ($200\ \mu L\ L^{-1}$). Initially, carbon fractionation under high $[CO_2]$ was high (20–29‰) and remained high after the transfer to low $[CO_2]$ conditions even as the rate of photosynthesis fell to 25% of the original rate. Carbon isotope discrimination decreased over the following 3 h to ~ 4‰, with respect to the carbon isotopic composition of CO_{2g}, as the rate of photosynthesis increased. Importantly, when the activity of carbonic anhydrase was chemically suppressed, the rate of photosynthesis decreased while ^{13}C discrimination increased. These results clearly indicate that *C. reinhardtii* has the capacity to enhance carbon availability when $[CO_{2aq}]$ is limiting and, by doing so, alter the isotopic character of the organic carbon produced.

In general, diatoms have demonstrated a capacity to increase the concentration of intercellular dissolved inorganic carbon ([DIC]) relative to ambient concentrations. The carbon uptake pathway of diatom assemblages, characterized by large-diameter diatoms including *Asterionella*, *Nitzchia* and *Rhizoslenia* from the Delaware Bay, were studied using ^{14}C-labelled HCO_3^- [103]. These

uptake experiments demonstrate that diatoms utilize newly introduced HCO_3^- within 10 s, increasing intercellular [DIC] up to ten times that of ambient concentrations and supporting high photosynthetic rates at low ambient [DIC]. The specific mechanism of carbon transport could not be clearly determined. Inhibition of carbonic anhydrase activity had little effect on intercellular [DIC], but led to a decrease in carbon fixation. These results allow the possibility that HCO_3^- is actively transported across the plasmalemma, while carbonic anhydrase is used to catalyse the dehydration of HCO_3^- within the cell [103].

Laws et al. [96] provided organic isotope evidence for a carbon concentrating mechanism in the diatom *P. tricornutum*. Under very low [CO_{2aq}] (< 2.4 μmol kg^{-1}), the relationship between ε_p and $\mu/[CO_{2aq}]$ for *P. tricornutum* deviates from linearity (Fig. 4) as a result of high growth rates and low carbon isotope fractionation. This non-linearity is consistent with either active uptake of HCO_3^- or CO_{2aq} or the catalysed addition of extracellular CO_2 leading to an increased diffusive flux [96].

Other culture experiments suggest that different growth and environmental conditions trigger different carbon uptake pathways, as well as carbon isotopic responses [104]. For example, strains of *E. huxleyi*, *P. tricornutum* and *P. glacialis*, grown in dilute batch cultures under nitrate-replete conditions and varying light/dark cycles, demonstrate that although ε_p varies with respect to [CO_{2aq}] and $\mu/[CO_{2aq}]$, these relationships differ from those established in nutrient-limited, predominantly continuous light, chemostat incubations [105]. Relative to chemostat cultures, dilute batch cultures result in substantially lower absolute ε_p values, and different, as well as non-linear, species-specific slopes for ε_p versus $\mu/[CO_{2aq}]$ (Fig. 5).

Low ε_p values associated with carbon-concentrating mechanisms are likely a consequence of reservoir effects. Francois et al. [106] argued that ε_p is

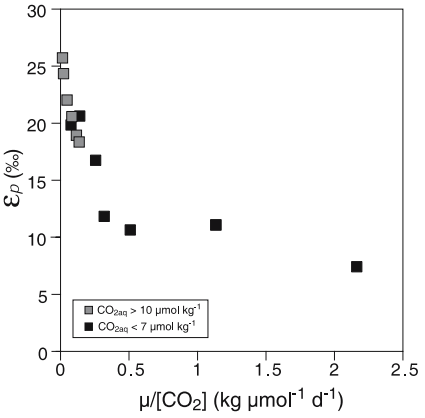

Fig. 4 The effect of low [CO_{2aq}] on *P. tricornutum* determined from chemostat incubations. [CO_{2aq}] > 10 μmol kg^{-1}: *filled squares*; [CO_{2aq}] < 7 μmol kg^{-1}: *shaded squares* [211]

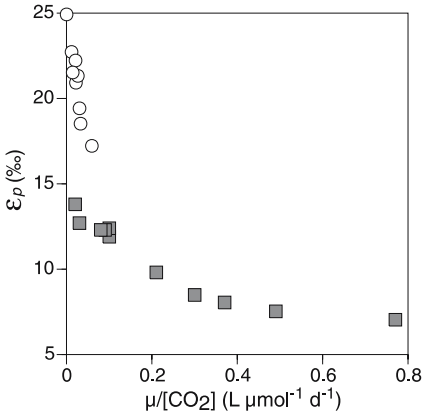

Fig. 5 Cultures of *E. huxleyi*: ε_p versus $\mu/[CO_{2aq}]$ from chemostat incubations and dilute batch cultures. Chemostat incubations: *open circles* [90], conducted under nitrate-limited, continuous light conditions. Dilute batch cultures: *shaded squares* [105], performed under nitrate-saturated, 16 : 8-h light/dark regime

a function of the fraction of intercellular inorganic carbon that diffuses back into the environment:

$$\varepsilon_p = \varepsilon_t + f(\varepsilon_f - \varepsilon_t) \tag{12}$$

where f is the fraction of the total intercellular carbon that back-diffuses from the cell. Low ε_p values suggest that the internal reservoir of CO_2 is finite with a low back-diffusive flux. Depletion of the internal carbon reservoir leads to a Rayleigh-type fractionation that drives the product (i.e. organic carbon) to approach the isotopic composition of the reactant (i.e. CO_{2aq}). Other considerations include the form of inorganic carbon transported. If HCO_3^- is actively transported and completely catalysed intercellularly, the $\delta^{13}C$ value of the source CO_{2aq} would be approximately 8‰ enriched in ^{13}C with respect to ambient CO_{2aq} and consequently lead to lower apparent ε_p values. Although the culture experiments for *P. tricornutum* yielded low ε_p values associated with low $[CO_{2aq}]$ and high growth rates, Laws et al. [96] found that Eq. 11 (based on Eq. 12) did not fit their experimental results. Considering the additional energetic expense associated with active uptake, the authors constructed a model that allows for both passive and active transport of inorganic carbon while providing a minimal energetic cost to the organism:

$$\frac{\mu}{C_e - C_o} = \frac{k_{-1}}{C(1+\beta)}\left(\frac{\varepsilon_2' - \varepsilon_p}{\varepsilon_p - \varepsilon_1'}\right) \tag{13}$$

where $\varepsilon_2' = \varepsilon_2 - \varepsilon_{-1} + \varepsilon_1$, and $\varepsilon_1' = \varepsilon_1 + (\beta/(1+\beta))(\varepsilon_2 - \varepsilon_{-1})$, and β and C_o are constants. ε_2, ε_1 and ε_{-1} represent the fractionations associated with carbon fixation, and transport into and out of the cell, respectively.

4
Controls on Higher Plant $\delta^{13}C$ Values

Higher plant biomass, including specific biomarkers, is common in marine sediments. Like those of algal biomass, higher plant $\delta^{13}C$ values are governed by the isotopic composition of substrate carbon, fractionation during carbon assimilation (ε_p) and environmental conditions that influence ε_p values. In addition, higher plant physiology, specifically the differences between C_3 and C_4 plants, exerts an important control on their carbon isotopic compositions.

4.1
The Carbon Isotopic Composition of Atmospheric Carbon Dioxide

The majority of higher plant lipids found in marine or lacustrine sediments are thought to derive from sub-aerial land plants rather than submerged plants. Thus, atmospheric carbon dioxide is their sole carbon source and controls on the $\delta^{13}C$ values of atmospheric CO_2 represent a major control on the carbon isotopic compositions of higher plants. In the recent past, the primary control on atmospheric CO_2 $\delta^{13}C$ values has been the burning of fossil fuels—the Suess effect—which has caused CO_2 to become ca. 1.5‰ more depleted in ^{13}C since the industrial revolution [107]. Prior to that, atmospheric CO_2 $\delta^{13}C$ values appear to have varied little in the recent past; since the last glacial period maximum values have varied from – 6.4 to – 6.9‰ despite significant changes in CO_2 concentrations. On longer timescales, atmospheric CO_2 $\delta^{13}C$ values have changed along with the entire ocean–atmosphere reservoir, as discussed above. In addition to these global changes, the carbon isotopic composition of air in a plant's immediate growth environment can differ. An example of this is the canopy effect [108], wherein ^{13}C-depleted CO_2, generated by soil respiration, accumulates and is assimilated into plants growing below the forest canopy. Similarly, ^{13}C-depleted CO_2 derived from methane oxidation has been invoked to explain variations in peat bog vegetation $\delta^{13}C$ values [109].

4.2
The Carbon Isotopic Compositions of C_3 Plants

The majority of extant and fossil vascular plants are characterized by C_3 physiology, and various studies have established that photosynthetic fixation of atmospheric CO_2 by plants is accompanied by significant discrimination against ^{13}C [110]. As with aquatic photoautotrophs, the primary cause of photosynthetic carbon isotope fractionation during C_3 plant photosynthesis is the discrimination against ^{13}C by rubisco during carboxylation of ribulose-1,5-bisphosphate. Also in common with aquatic photoautotrophs, numerous studies have revealed that $\delta^{13}C$ values of C_3 plants vary significantly.

The carbon isotopic composition of C_3 plants is related to that of atmospheric CO_2 by Eq. 10, described above for aquatic photoautotrophs, and is contingent upon the same assumptions as described above. Distinct from aquatic photoautotrophs, however, the carbon isotope fractionation associated with diffusive transport (ε_t) is estimated to be 4.4‰; the carbon isotope fractionation during carboxylation mediated by rubisco (ε_f) is generally thought to be ca. 30‰. As with microalgae, Eq. 10 indicates that if the $\delta^{13}C_{air}$ value increases or the C_i/C_a ratio decreases, the $\delta^{13}C$ value of plant tissues increases. On geological timescales, the most important control on C_i/C_a ratios in higher plants is atmospheric pCO_2 [11]; lower pCO_2 levels result in low C_i/C_a ratios and lower plant $\delta^{13}C$ values. However, higher plant $\delta^{13}C$ values are not as useful a palaeo-pCO_2 barometer as those of algal-derived organic matter, because the latter organisms are effectively more carbon-limited by slow CO_2 diffusion in water [11]. C_i/C_a ratios also decrease if stomatal conductance in the plant leaf is reduced, which can occur at low humidity to minimize loss of water via evapotranspiration [95, 111]. Indeed, reduced water availability associated with low precipitation or hypoxic soil correlates with higher $\delta^{13}C$ values in different Hawaiian populations of a single C_3 species [112].

The rate of carbon assimilation, reflecting the plant's growth rate but also specific rates at individual leaves, will also affect C_i/C_a ratios and plant $\delta^{13}C$ values [113, 114], although this has not been as well-studied as for algae. Controls on carbon assimilation rates include nutrient status and light intensity; while the former probably influences the entire plant, it is possible that $\delta^{13}C$ values could vary among leaves on a single plant depending on their orientation with respect to the sun. Indeed, Lockheart et al. [115] observed that leaves on the southern side of (northern hemisphere) trees were enriched in ^{13}C relative to leaves on the northern side of the same tree and attributed this difference to enhanced rates of photosynthesis in the south-facing leaves. Temperature is expected to exert a minor control on isotopic fractionation by the rubisco enzyme [116, 117]; this has been demonstrated by in vitro studies [118] and some field investigations [119–122], while others have failed to find any effect [110]. However, the relationship between temperature and fractionation varies widely in both magnitude and sign, probably due to the difficulty in resolving multiple variables. Imposed on these environmental controls, there appear to be significant ecosystem and interspecies variations in $\delta^{13}C$ values among C_3 plants. For example, Chikaraishi and Naraoka [123] observed that C_3 angiosperm species are depleted in ^{13}C relative to co-occurring C_3 gymnosperms (-32.8 ± 2.5‰ and -26.9 ± 1.1‰, respectively).

4.3 C_3 vs. C_4 Plants

In contrast to C_3 plants, C_4 plants initially fix carbon as bicarbonate via carboxylation of phosphoenolpyruvate [110], forming oxaloacetate (Fig. 6).

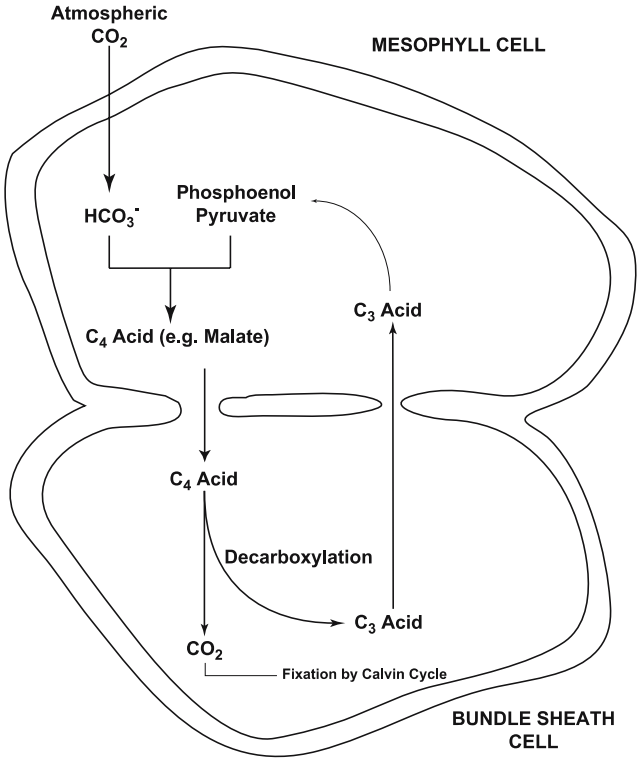

Fig. 6 Schematic of a C_4 plant mesophyll and bundle sheath cells and how carbon is shuttled between them

This occurs in the outer layer of photosynthetic cells (mesophyll), and the fixed carbon, as either malate or aspartate, is transported to the inner bundle sheath cells where decarboxylation occurs, ultimately regenerating phosphoenolpyruvate and releasing CO_2. Critically, it is thought that all of this released CO_2 is then fixed by rubisco. Because fractionation by phosphoenolpyruvate carboxylase is small (2.2‰), and the complete utilization of CO_2 in the bundle sheath results in no expression of the isotope effect associated with rubisco-mediated carboxylation, the net fractionation during C_4 photosynthesis is very small (– 1.3‰) [124]. Numerous studies have confirmed that C_4 plant biomass (– 10 to – 16‰) is significantly enriched relative to that of C_3 plants (– 25 to – 30‰). Moreover, $\delta^{13}C$ values for C_4 plants are much less dependent on the C_i/C_a ratio and environmental variables than those for C_3 plants [124]. The fact that C_3 and C_4 plants can be distinguished through their $\delta^{13}C$ values is of great use in palaeoclimatic investigations. C_3- and C_4-type plants have different optimum conditions for growth, and it is generally thought that high temperatures and low pCO_2 favour C_4-dominated ecosystems [125].

5
Controls on Prokaryote $\delta^{13}C$ Values

Prokaryotes inhabit a vast range of environments and have diverse metabolisms, ranging from methanogenesis to photoautotrophy to heterotrophy; consequently, their $\delta^{13}C$ values are much more variable than those of eukaryotes.

5.1
The Carbon Isotopic Composition of Microbial Substrate Carbon

Carbon substrates for bacterial and archaeal growth include CO_{2aq}, HCO_3^-, CH_4 and a variety of low molecular weight organic compounds. For autotrophic organisms utilizing either CO_{2aq} or HCO_3^-, the same controls on DIC $\delta^{13}C$ values discussed for aquatic photoautotrophs are applicable. However, bacterial and archaeal autotrophs include chemoautotrophs, which are not dependent on sunlight, and they occupy a far greater range of environmental settings—including shallow and deep marine sediments and the water column—than photoautotrophs. In such settings, DIC $\delta^{13}C$ values can vary significantly; near cold seeps or in organic-rich sediments, where a significant quantity of DIC is ultimately derived from oxidation of methane or organic matter, DIC is more ^{13}C-depleted [126]. In contrast, in closed or semi-closed settings, autotrophic, and particularly methanogenic, assimilation of DIC can cause the residual pool to become enriched in ^{13}C [126, 127].

Methane $\delta^{13}C$ values are generally strongly depleted in ^{13}C [126] and methanotroph lipids and biomass have lower $\delta^{13}C$ values—often lower than – 100‰ [128]—than any other organic material. However, methane $\delta^{13}C$ values are also quite variable, depending on (1) whether the methane is thermogenic or biogenic and (2) if biogenic, whether methane was generated autotrophically or heterotrophically and correspondingly, the carbon isotopic compositions of DIC or acetate [126]. However, extensive methane oxidation and resultant Rayleigh distillation also exert an important control on methane $\delta^{13}C$ values in the environment.

Microbial heterotrophs obviously make use of substrates with widely divergent $\delta^{13}C$ values depending on the ecology of the source organism(s). For example, lipids of inferred bacterial heterotrophs living in methane-oxidizing environments have low $\delta^{13}C$ values [129]. In addition, different substrates (glucose, acetate) derive from different biosynthetic pathways in the source organism and this can impart different carbon isotopic compositions to the consumer. For example, carbohydrates are typically enriched in ^{13}C relative to lipids [130–133]. The $\delta^{13}C$ values of substrates generated from the degradation of these different compound classes vary widely, and thus heterotrophic microorganisms will reflect those differences. Indeed, preferential utilization of carbohydrate-derived carbon has been invoked as an explanation for ^{13}C-enriched bacterial lipids in peats [129, 134] and soils [135].

5.2 Isotope Fractionation During Carbon Assimilation by Bacteria and Archaea

Unlike eukaryotic photoautotrophs, all of which utilize the Calvin cycle during carbon assimilation, bacteria and archaea employ a wide range of carbon assimilation mechanisms. Many chemoautotrophs utilize the Calvin cycle and, thus, rubisco as the carboxylating enzyme, although studies of this are limited [136, 137]. Rubisco-catalysed carboxylation appears to have a similar fractionation (27‰) in bacteria and archaea as in eukaryotic photoautotrophs. Other pathways, apparently restricted to the bacteria and archaea, are the reverse tricarboxylic acid (TCA) cycle, the carbon assimilation pathway utilized by the green sulphur bacterium *Chlorobium* [138, 139], and the 3-hydroxypropionate pathway, utilized by the green non-sulphur bacterium *Chloroflexus* [140, 141] as well as some archaea [142].

The reverse TCA cycle involves a C_4 substrate, starting with oxaloacetate, to which two carbon atoms are sequentially added to form citrate; cleavage of citrate forms acetyl coenzyme A (acetyl-CoA), which is then carboxylated to pyruvate. Thus, in three discrete steps, two of which are catalysed by reduced ferredoxin, a total of three carbon atoms are assimilated. Critically, none of the carboxylations is apparently characterized by a large carbon isotopic fractionation and the net fractionation is much lower than for organisms using the Calvin cycle. Sirevåg et al. [138] reported $\Delta\delta^{13}C$ values ($\delta^{13}C_{biomass} - \delta^{13}C_{CO_2} \sim \varepsilon_p$) of 2.5 to 5.2‰, while Quandt et al. [139] reported $\Delta\delta^{13}C$ values of 12.2‰. Similar low values for the reverse TCA cycle have been observed for non-photoautotrophic organisms utilizing this pathway [137, 143].

The 3-hydroxypropionate pathway [140, 141] involves two carboxylations of acetyl-CoA to form methylmalonyl-CoA, which is then rearranged and cleaved to regenerate the acetyl-CoA and yield glyoxylate. The 3-hydroxypropionate pathway is also characterized by relatively low carbon isotopic fractionation, with Holo and Sirevåg [140] observing a 14‰ difference between biomass and dissolved inorganic carbon and van der Meer et al. [144] observing a 12.2‰ difference. It is thought that one reason for the low carbon isotope fractionation relative to DIC is that *Chloroflexus* might assimilate bicarbonate rather than dissolved CO_2 [144], consistent with the presence of the PEP carboxylase enzyme [142]. Organisms other than *Chloroflexus* that use the 3-hydroxypropionate pathway also exhibit low carbon isotope fractionation during carbon assimilation [137, 142] (0.6 to 3.2‰ relative to CO_{2aq}), and utilization of this pathway has been invoked to explain the ^{13}C-enriched composition of pelagic crenarchaeal lipids [145, 146].

There is relatively little known about the controls on the carbon isotopic composition of methanogenic archaea. Methanogens assimilate either CO_2 or other C_1 substrates (methylotrophs) or acetate, and it has generally been thought that such organisms will have a highly ^{13}C-depleted biomass, similar

to the low $\delta^{13}C$ values of generated methane. This has been shown for several species of methanogens utilizing C_1 substrates grown in culture [147], and has been invoked as an explanation for ^{13}C-depleted isoprenoids in the Messel Shale [13]. However, methanogen biomarkers found in a variety of other settings, including Ace Lake, Antarctica [148] and peats [134], tend to have $\delta^{13}C$ values similar to or even enriched relative to those of co-occurring plant biomarkers. Potentially, this reflects reduced carbon isotope fractionation during acetate utilization [134] or complete utilization of the substrate pool in a closed system [147].

Methanotroph $\delta^{13}C$ values can be similarly variable. As with autotrophs, significant but variable kinetic carbon isotope effects are associated with methane assimilation [149]. Jahnke et al. [149] showed that methanotroph biomass $\delta^{13}C$ values can be as much as 24.8‰ depleted relative to substrate methane, but also observed 30‰ variability depending on whether the methanotrophs utilized the ribulose monophosphate or serine pathways and whether they used the membrane-bound particulate monooxygenase enzyme or the soluble isozyme. Combined with the low $\delta^{13}C$ values typical of methane, this results in the methanotroph biomass being highly depleted in ^{13}C. Methane is also the carbon substrate for anaerobic methane-oxidizing archaea [128, 150, 151]. These organisms have not yet been isolated and the mechanism that they employ for methane uptake is unknown. Environmental studies where biomarker and methane $\delta^{13}C$ values have both been determined are uncommon and should be interpreted with caution due to the spatial and temporal variability of the latter, but these studies do suggest that lipids of methane-oxidizing archaea can be 10 to 55‰ depleted relative to the methane substrate [150, 152].

In contrast to multicellular heterotrophs in which respiratory loss of carbon can be significant, prokaryotic heterotroph carbon isotopic compositions are generally thought to be similar to that of the food [14]. However, laboratory incubations of *Shewanella putrefaciens* by Teece et al. [153] revealed that small differences (< 2.5‰) between substrate and biomass $\delta^{13}C$ values can occur and are dependent on the growth conditions. More strikingly, recent work on the iron-reducing bacteria, *Geobacter metallireducens* and *Shewanella algae*, indicates that these heterotrophs' biomass can be as much as 7‰ depleted relative to substrate acetate and lactate, respectively [154]. Thus, assumptions that the bacterial heterotroph biomass will always be the same as that of substrate carbon need to be more thoroughly tested.

6 Biosynthetic Controls on Lipid $\delta^{13}C$ Values

After carbon assimilation, isotope effects during biosynthesis further affect the $\delta^{13}C$ values of specific lipids within an organism. This can cause differ-

ences in $\delta^{13}C$ values among compound classes (e.g. lipids vs. carbohydrates as described above) and also between $\delta^{13}C$ values of individual lipids within a structural class. The traditional paradigm regarding biosynthetic isotope effects is that fractionation occurs during formation of acetyl-CoA with the strongest depletion occurring at the carboxyl carbon [155]; presumably this fractionation is associated with either the oxidation of pyruvate to acetyl-CoA by pyruvate dehydrogenase [156] or conversion of acetyl phosphate to acetyl-CoA by phosphotransacetylase [157]. Monson and Hayes [155] determined that the kinetic isotope effect associated with pyruvate dehydrogenase in *E. coli* was 23‰ (ε_{PDH}), but this full effect is rarely expressed because of Rayleigh distillations (such that the residual pyruvate carbon pool becomes progressively enriched in ^{13}C as the reaction progresses). Instead, the fractionation expressed during decarboxylation is $(1 - f)\varepsilon_{PDH}$ [155], where f is the fraction of pyruvate flowing to acetyl-CoA.

Because these reactions occur during both photoautotrophic and heterotrophic lipid synthesis, acetogenic lipids in most organisms are expected to be ca. 4‰ depleted relative to biomass [14]. Isoprenoids synthesized by the mevalonic acid pathway, which results in a 3 : 2 ratio of methyl to carboxyl atoms, are expected to be depleted relative to biomass by only ca. 2‰. However, it is now recognized that isoprenoids are not synthesized via the mevalonic acid pathway in many or most organisms; instead, the C_5 isoprene unit can be formed by condensation of a C_2 subunit derived from pyruvate decarboxylation and a C_3 subunit derived from triose phosphate [158–161]. This pathway actually appears to be predominant in bacteria and has also been identified in higher plants [162], unicellular algae, and cyanobacteria [163]. The effect of the glyceraldehyde phosphate/pyruvate pathway on the carbon isotopic composition of isoprenoids remains unclear. It is possible that isoprenoids derived from this pathway could be enriched in ^{13}C relative to mevalonate-derived isoprenoids, because the former contain only one ^{13}C-depleted carboxyl carbon.

Generally, biomarker lipid $\delta^{13}C$ values tend to match these general considerations, but significant exceptions are common. In the following sections, we discuss algal, higher plant and prokaryotic biomarker $\delta^{13}C$ values in the context of the above considerations.

6.1 Microalgae

The carbon isotopic compositions of microalgae have been studied by a number of workers. In general, they exhibit relationships with bulk organic matter similar to those described above, but there are a number of exceptions and the range of values can be considerable. Bidigare et al. [90] reported that alkenones were 3.8‰ depleted in ^{13}C relative to haptophyte biomass, and subsequent work has generally agreed with that finding. However, Schouten

et al. [164] showed that the offsets between lipid and bulk organic matter $\delta^{13}C$ values in microalgal batch cultures are quite variable. In general, fatty acid $\delta^{13}C$ values varied by ca. 2‰ within a given organism; however, the fatty acids ranged from 0.8 to 8.7‰ depleted relative to bulk biomass. Alkenones in *Isochrysis galbana* generally had $\delta^{13}C$ values 3 to 3.5‰ depleted relative to biomass consistent with the work of Bidigare et al. [90], but were enriched by 4 to 4.5‰ relative to fatty acids, ostensibly derived from similar biosynthetic pathways. Isoprenoidal lipids, phytol and sterols had $\delta^{13}C$ values consistent with theoretical predictions, being enriched relative to fatty acids and depleted relative to bulk biomass, but their values ranged from being nearly the same as biomass to being > 8‰ depleted relative to it. Evaluating the isotopic offset between lipids and biomass is harder to do in field investigations due to the range of compounds and organisms that contribute to particulate organic matter. Consequently, a range of differences have been observed. In the Peru upwelling region [90, 165], alkenones, phytol and a variety of sterols inferred to derive from sterols are depleted relative to particulate organic carbon (POC) $\delta^{13}C$ values by typically 1 to 4‰, but no systematic offset is observed between alkenones and isoprenoids. In contrast, Popp et al. [166] observed differences of 5 to 12‰ between $\delta^{13}C$ values of POC and steroids thought to derive from diatoms. More recent work has reported biomass–lipid offsets falling between these two extremes, further illustrating that the controls on lipid $\delta^{13}C$ values are complex and their relationship to bulk organic carbon $\delta^{13}C$ values is still poorly understood.

6.2 Higher Plants

n-Alkanes are the terrestrial biomarkers that have been most thoroughly characterized isotopically. Collister et al. [167] observed that in C_3 and C_4 species, the *n*-alkanes were depleted relative to biomass by ca. 5.9 and 9.9‰, respectively. *n*-Aldehydes had isotopic compositions similar to those of the *n*-alkanes, and it is thought that other biosynthetically related *n*-alkyl compounds (e.g. *n*-acids and *n*-alkanols) have similar $\delta^{13}C$ values. Chikaraishi and Naraoka [123] observed similar differences between biomass and *n*-alkane $\delta^{13}C$ values in a range of C_3 angiosperms and gymnosperms and C_4 plants. Lignin-derived phenols are depleted in ^{13}C compared to bulk plant tissue, but not to the same extent as lipids. Goñi and Eglinton [168] measured the $\delta^{13}C$ values of lignin phenols (produced from the oxidation of lignin polymers), and found that those from C_3 plants had $\delta^{13}C$ values of -30.4 ± 3.9‰ and those from C_4 plants had $\delta^{13}C$ values of -16.9 ± 2.7‰.

6.3 Prokaryotes

In general, a 2 to 4‰ offset between fatty acids and biomass is observed for bacteria grown under aerobic conditions, including *E. coli* grown on glucose [155], *S. putrefaciens* [153], and Type I and Type X methanotrophs using the ribulose monophosphate pathway (RuMP) [149, 169]. However, the fatty acids of cultured methanotrophs utilizing the serine pathway can be 10 to 15‰ depleted relative to biomass [149]. The acetogenic lipids of heterotrophic bacteria are also more depleted than expected when grown under anaerobic conditions, with fatty acid $\delta^{13}C$ values being: 7.3 to 10.7‰ more depleted than biomass in *S. putrefaciens* grown on lactate and with NO_3 as the oxidant [153]; 4.5 to 8.6‰ more depleted than biomass in *G. metallireducens* grown on acetate [154]; and 10.4 to 14.7‰ more depleted than biomass in *S. algae* grown on acetate [154].

The isotopic relationships between lipids and biomass can also vary in autotrophic prokaryotes. Theoretical considerations and culture studies indicate that in organisms using the reverse TCA cycle, such as green sulphur bacteria, acetogenic lipids are ca. 4‰ enriched in ^{13}C relative to biomass [170]. In contrast studies of *Chloroflexus aurantiacus* grown photoautotrophically indicate that alkyl lipids of organisms using the 3-hydroxypropionate pathway are 1 to 2‰ depleted in ^{13}C relative to biomass [132]. This is to be expected because these organisms also use the TCA cycle during lipid synthesis, such that the isotopic difference between biomass and lipids should be much the same as in photoautotrophs using the Calvin cycle.

As mentioned earlier, isotope fractionations are also dependent on partitioning of carbon at branch points in carbon metabolic pathways [14]. This is particularly well illustrated by culture studies of the cyanobacterium *Synechocystis* [171]. This organism uses the TCA cycle and lipids are biosynthesized from acetyl-CoA generated by decarboxylation of pyruvate, so that acetogenic lipids are expected to be ca. 4‰ depleted relative to biomass. Instead, Sakata et al. [171] observed that fatty acids were depleted by 9.1‰. This additional depletion suggests that the fraction of pyruvate flowing to acetyl-CoA is small, which is consistent with the relatively low abundance of lipids in cyanobacteria.

Different carbon assimilation pathways and mechanisms of acetyl-CoA formation will also affect isoprenoid lipid $\delta^{13}C$ values. For example, in the study by Jahnke et al. [169], hopanoids in methanotrophs utilizing the serine pathway had low $\delta^{13}C$ values similar to those of the fatty acids. Thus, although paradigms for the biosynthetic controls on lipid $\delta^{13}C$ values can provide a first approximation of expected biomarker $\delta^{13}C$ values in some situations, unresolved issues regarding the magnitude of isotopic effects, the influence of growth conditions and the biological distribution of different metabolic pathways remain a limitation in interpreting sedimentary lipid $\delta^{13}C$ values.

7 Applications

7.1 Alkenone $\delta^{13}C$ Values as a Paleo-pCO_2 Proxy

The stable carbon isotopic compositions of C_{37} di-unsaturated alkenones collected from surface waters across a range of oceanic environments have been studied in relationship to CO_2, nutrients, and other variables [34, 90, 100, 104, 172]. The influence of growth rate and cell geometry on ε_p values (see Eq. 5) derived from C_{37} di-unsaturated alkenones ($\varepsilon_{p37:2}$) are, however, difficult to evaluate given that these data are rarely, if ever, collected for specific species in natural settings. Therefore, the model described in Eq. 11 is not applicable in the analysis of field-based $\varepsilon_{p37:2}$ values. Instead, these data are commonly assessed using a convention proposed by Rau et al. [173] and Jasper et al. [174] and further modified by Bidigare et al. [90]:

$$\varepsilon_p = \varepsilon_f - \frac{b}{CO_{2aq}} \tag{14}$$

where b represents an integration of the physiological variables, such as growth rate and cell geometry, affecting the total carbon isotope fractionation during photosynthesis [90, 174].

The available data provide evidence for a significant correlation between the physiological-dependent term b and the concentration of reactive soluble phosphate (Fig. 7). It is likely that this relationship stems from the influence

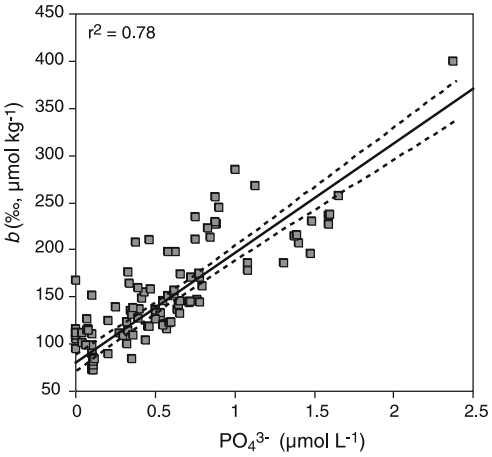

Fig. 7 Compilation of b versus soluble phosphate for natural haptophyte populations [34, 91, 100, 172, 212]. Values for b are calculated using a value of 25‰ for ε_f. *Solid line*: geometric mean regression; *dotted lines*: 95% confidence intervals

of growth rate on the expression of $\varepsilon_{p37:2}$ [90]. However, it is unlikely that $[PO_4^{3-}]$ alone is responsible for the variability in growth rate inferred from variation in *b*. Instead, Bidigare et al. [90] and Laws et al. [104] propose that the availability of specific trace elements, such as Se, Co and Ni, is ultimately impacting on the growth characteristics of natural haptophyte populations. In this sense, $[PO_4^{3-}]$ is acting as a proxy for these growth-limiting trace elements that also exhibit phosphate-like distributions in the modern ocean.

The robust relationship between $[PO_4^{3-}]$ and the physiologically dependent term *b* determined from $\varepsilon_{p37:2}$ values provides the opportunity to apply alkenone $\delta^{13}C$ values in the reconstruction of ancient CO_2 levels. That is, *b* can be cast in terms of $[PO_4^{3-}]$ and applied to Eq. 11 [12, 90, 104]. If phosphate concentrations can be constrained for a specific location and ancient values of $\varepsilon_{p37:2}$ reconstructed, CO_{2aq} concentrations can be estimated. In general, ancient $\varepsilon_{p37:2}$ records can be reconstructed by measuring the carbon isotopic composition of di-unsaturated alkenones and coeval near surface-dwelling planktonic foraminifera. The $\delta^{13}C$ values of foraminiferal carbonate are then used to estimate the $\delta^{13}C$ of CO_{2aq} in equilibrium with calcite. This approach was developed by Jasper and Hayes [175] and applied to evaluate palaeoceanographic dynamics and surface-water $[CO_{2aq}]$ during the Pleistocene [174]. These earlier studies calibrated $\varepsilon_p - CO_2$ relationships from measurements of particulate organic carbon in the modern ocean, derived primarily from highly productive waters. Subsequent studies have applied $\varepsilon_{p37:2}$ values in conjunction with phosphate estimates to reconstruct Late Quaternary surface water pCO_2 in the South Atlantic [176] and global Miocene-age pCO_2 trends [12, 177].

The alkenone–pCO_2 proxy rests on the assumption that intercellular CO_{2aq} fixed during photosynthesis arrives by diffusive flux, or that the proportion of diffusive and actively transported carbon flux is constant under a variety of environmental conditions. Results from chemostat culture experiments lend support to, but do not prove, a photosynthetic diffusion model for *Emiliania huxleyi*, the dominant haptophyte in the modern ocean [91]. The presence of carbonic anhydrase (CA) was not found in low-calcifying strains of *E. huxleyi* [178], but CA was detected in the chloroplasts of high-calcifying cells [179]. Inhibition of CA activity led to only a 30% decrease in $^{14}CO_2$ fixation, suggesting that a CA-mediated carbon flux constitutes a minor contribution to the overall inorganic carbon flux [179]. Further, there appear to be differences between exponential versus stationary growth phases for *E. huxleyi*. During the stationary phase *E. huxleyi* appears to maintain substantially higher intercellular DIC concentrations relative to ambient levels, suggesting that stationary-phase cells have the capacity to transport inorganic carbon against a concentration gradient [180].

Many, if not most, marine microalgae demonstrate characteristics of a carbon concentrating mechanism. This includes haptophytes such as *Isochrysis*

galbana [89, 102], as well as stationary-phase cells of high-calcifying strains of *E. huxleyi* [180]. Moreover, batch cultures suggest that carbon isotope fractionation may be influenced differently by light-limited [105, 181] versus nutrient-limited growth performed in chemostat experiments [90]. Whether or not haptophyte populations in their natural settings control intercellular concentrations of inorganic carbon by actively transporting bicarbonate or CO_{2aq} remains unresolved.

Recently, Pagani et al. [182] tested the accuracy of the alkenone $\varepsilon_p - CO_2$ technique by comparing reconstructed pre-industrial water-column $[CO_{2aq}]$ from sedimentary alkenone $\delta^{13}C$ values from 20 sites across a North Pacific transect against both observed water-column $[CO_{2aq}]$ values and estimated pre-industrial concentrations at the depth of alkenone production at each site. Sedimentary alkenone-based CO_{2aq} estimates ($[CO_{2aq}]_{alk}$) were established by estimating the depth of alkenone production at each site as defined by $U^{K'}_{37}$ temperature estimates [183] and seasonal temperature–depth relationships established by the northwest Pacific carbon cycle study [184]. Production depths inferred by these records (Fig. 8a) were then used to identify the appropriate $\delta^{13}C_{CO_{2aq}}$ values and phosphate concentrations (Fig. 8b) required in the calculation of ε_p and $[CO_{2aq}]_{alk}$.

The pattern of ε_p values across the Pacific transect (Fig. 9), that is, lower values in high-nutrient environments (high and low latitudes) and higher ε_p values in the oligotrophic subtropics, is consistent with a growth rate control on carbon isotope fractionation. Although $[CO_{2aq}]_{alk}$ values track measured water-column values, they are clearly lower than modern values across the subtropical region. This offset likely reflects the contributions of anthropogenic CO_2 in modern surface waters relative to pre-industrial concentrations at the time of alkenone production. The smallest offsets are observed at the higher latitudes, consistent with expectations, since in regions subjected to intense seasonal upwelling, a component of surface CO_{2aq} derives from deeper, pre-industrial waters. The offset is greater across well-stratified waters in the subtropical latitudes, which track the rise in anthropogenic CO_2 more closely. When a model-based estimate of anthropogenic CO_2 is removed from the modern observed values, a majority of the $[CO_{2aq}]_{alk}$ values fall within 20% of modelled pre-industrial values. Thus, both the magnitude and pattern of offset between pre-industrial $[CO_{2aq}]_{alk}$ and modern $[CO_{2aq}]$ are consistent with a 30% anthropogenic increase in pCO_2 over the past 150 years. When the effects of anthropogenic $[CO_{2aq}]$ are removed from the modern signal, alkenone CO_{2aq} estimates accurately reproduce pre-industrial water column concentrations (Fig. 10).

The results of Pagani et al. [182] support the use of alkenone-based ε_p values as a proxy for palaeo-pCO_2 reconstruction and suggest that the alkenone approach can resolve relatively small differences in water-column CO_2 when phosphate concentrations and temperatures are well constrained. Their

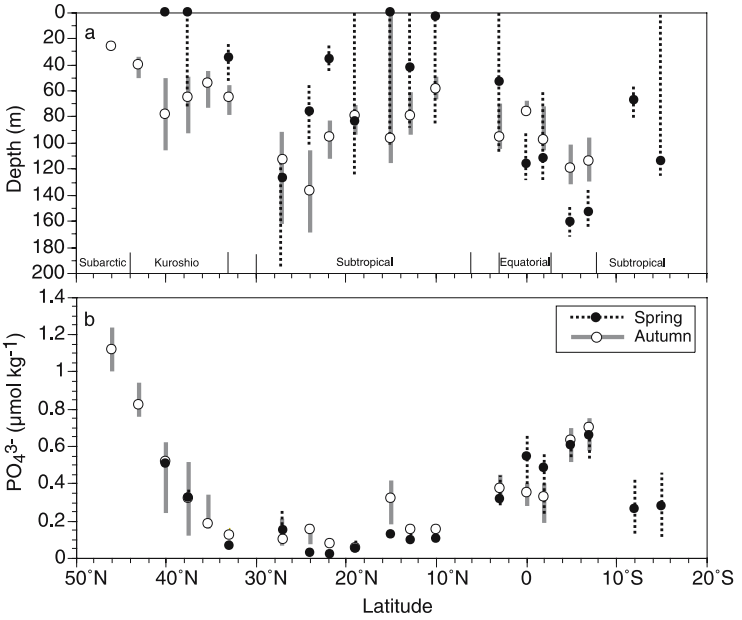

Fig. 8 Relationship between depth of haptophyte production and phosphate concentration across 175°E [182]. **a** Estimated seasonal depth of haptophyte production based on $U^{K'}_{37}$ temperature values and seasonal temperature–depth relationships established by NOPACCS. *Lines* represent the possible range of production based on $U^{K'}_{37}$ values ±1 °C; *squares* represent depths as defined by exact $U^{K'}_{37}$ values. Temperatures calculated using the results of Prahl et al. [213]. **b** Seasonal phosphate concentrations as defined by inferred haptophyte production depths and seasonal phosphate–depth relationships established by NOPACCS. *Open circles*: Autumn (August and September); *filled circles*: Spring (April, May and June)

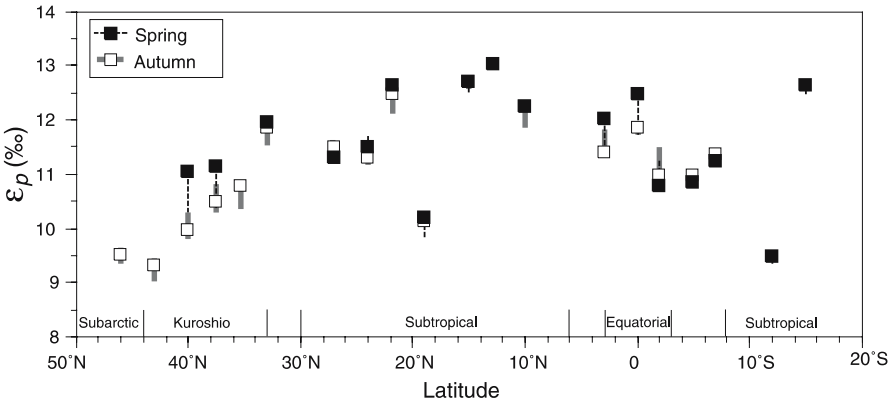

Fig. 9 $\varepsilon_{p37:2}$ values across 175°E reconstructed from sedimentary alkenones [182]. *Filled squares*: $\varepsilon_{p37:2}$ values assume Spring production. *Open squares*: $\varepsilon_{p37:2}$ values assume Autumn production

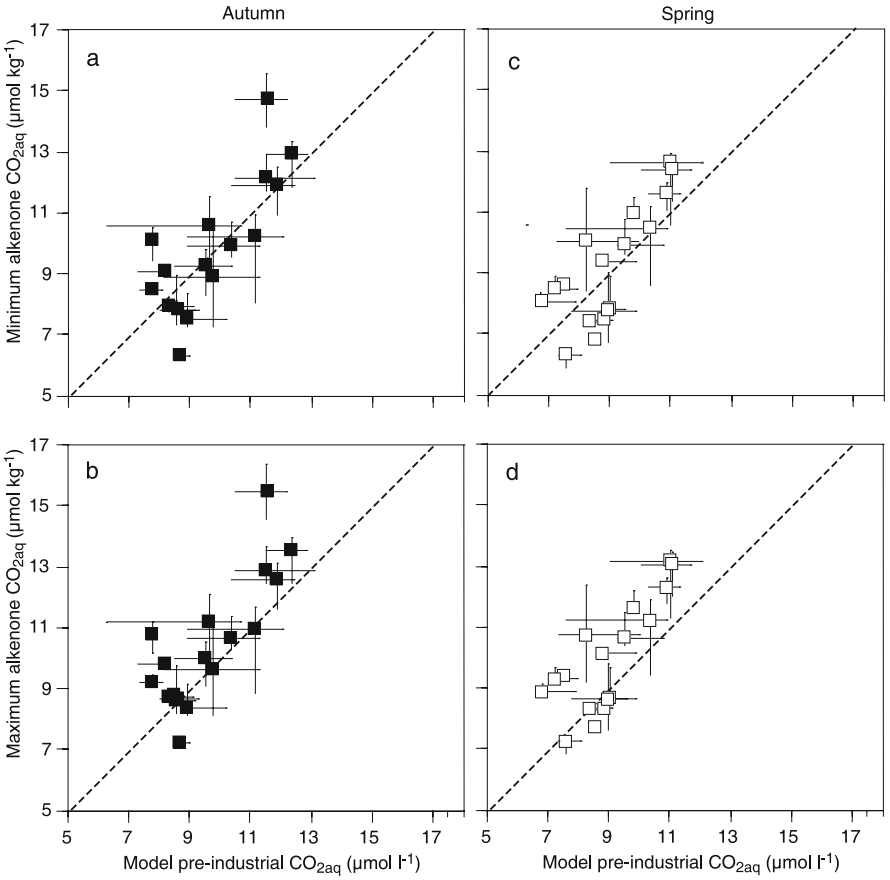

Fig. 10 Modelled pre-industrial [CO_{2aq}] versus alkenone-based [CO_{2aq}]. Crossplot of modelled pre-industrial [CO_{2aq}] versus minimum and maximum alkenone-based [CO_{2aq}]. **a**, **b** Autumn production assumed. **c**, **d** Spring production assumed. Maximum alkenone-based [CO_{2aq}] calculated using $\varepsilon_f = 27‰$ and the equation: $[CO_{2aq}] = (4.14[PO_4^{3-}] + 125.48[PO_4^{3-}] + 107.85)/(27 - \varepsilon_p)$. Minimum alkenone-based [CO_{2aq}] calculated using $\varepsilon_f = 25‰$ and the equation: $[CO_{2aq}] = (116.12[PO_4^{3-}] + 81.5)/(25 - \varepsilon_p)$. *Dashed line*: 1 : 1 correlation

results further suggest that light-limited growth effects and/or active carbon uptake are negligible, or that these processes have negligible effects on carbon isotopic compositions of haptophytes in the natural environment.

7.2 Identifying Methane Cycling in Modern and Ancient Settings

Due to the highly ^{13}C-depleted character of methane in most settings, biomass derived from organisms either directly or indirectly supported by

methane can be readily identified. Although this applies to all methane-utilizing organisms, in marine sediments it is particularly useful in examining anaerobic oxidation of methane (AOM). In marine environments, methane oxidation occurs under anaerobic conditions and is coupled to sulphate reduction [185–189]. Consequently, only a small proportion of the methane generated in marine sediments is available for aerobic oxidation and the flux of methane from marine sediments to the atmosphere is small compared to other sources [190]. Multiple lines of evidence show that in such diverse settings as Hydrate Ridge [77, 191], the California Margin [150], Mediterranean mud volcanoes [151], Gulf of Mexico hydrocarbon seeps [192, 193], Black Sea sediments [152, 194] and water column [195, 196], and the Guyamas Basin [197], methane is consumed anaerobically in a process mediated by archaea. Whilst the nature of the AOM community has subsequently been elucidated by a variety of microbial techniques, including 16S rRNA analyses [150, 198] and fluorescence in situ hybridization [191], the identification of ^{13}C-depleted diagnostic archaeal biomarkers was critical in confirming the role of archaea in AOM (Fig. 11). Among the archaeal biomarkers found at cold seep sites are archaeol, *sn*-2- and *sn*-3-hydroxyarchaeol, glycerol dialkyl glycerol tetraethers, pentamethylicosane and crocetane (and unsaturated analogues). The diversity of ^{13}C-depleted archaeal biomarkers amongst different sites has been proposed as evidence that multiple species of archaea mediate AOM.

^{13}C-depleted bacterial biomarkers have also been detected at cold seeps, providing insight into the co-existing bacterial community [151, 191, 198–203]. Apparently, some or all AOM archaea are unable to reduce sulphate during methane oxidation, and sulphate-reducing bacteria (SRB) are required to syntrophically consume accumulating reduced substrates [204] (acetate, formate, H_2) if AOM is to remain thermodynamically viable [205]. Consistent with this, highly ^{13}C-depleted C_{15} and C_{17} *iso* and *anteiso* fatty acids, common in bacteria but particularly abundant in SRB, are abundant in cold seep sediments. Other ^{13}C-depleted fatty acids are also commonly found in cold seep sediments and likely derive from SRB [203]. Also present are ^{13}C-depleted hopanoids and non-isoprenoidal dialkyl glycerol diether lipids [199, 201], the latter also inferred to be SRB biomarkers. While the bacterial biomarkers are all strongly depleted in ^{13}C relative to typical algal biomarkers, indicating that a significant portion of the carbon must derive from methane, Pancost et al. [129, 201], Hinrichs et al. [199] and Thiel et al. [152] have observed that they are 10 to 40‰ enriched relative to the co-occurring archaeal biomarkers (Fig. 12). Such differences have led to speculation about the nature of carbon flow amongst these syntrophic organisms. For example, the enrichment can be explained if the SRB are autotrophic and assimilating a mixture of seawater and methane-derived DIC [129].

In addition, archaeal and bacterial biomarkers can be used to identify related processes in ancient cold seep deposits. Among the ancient cold seep

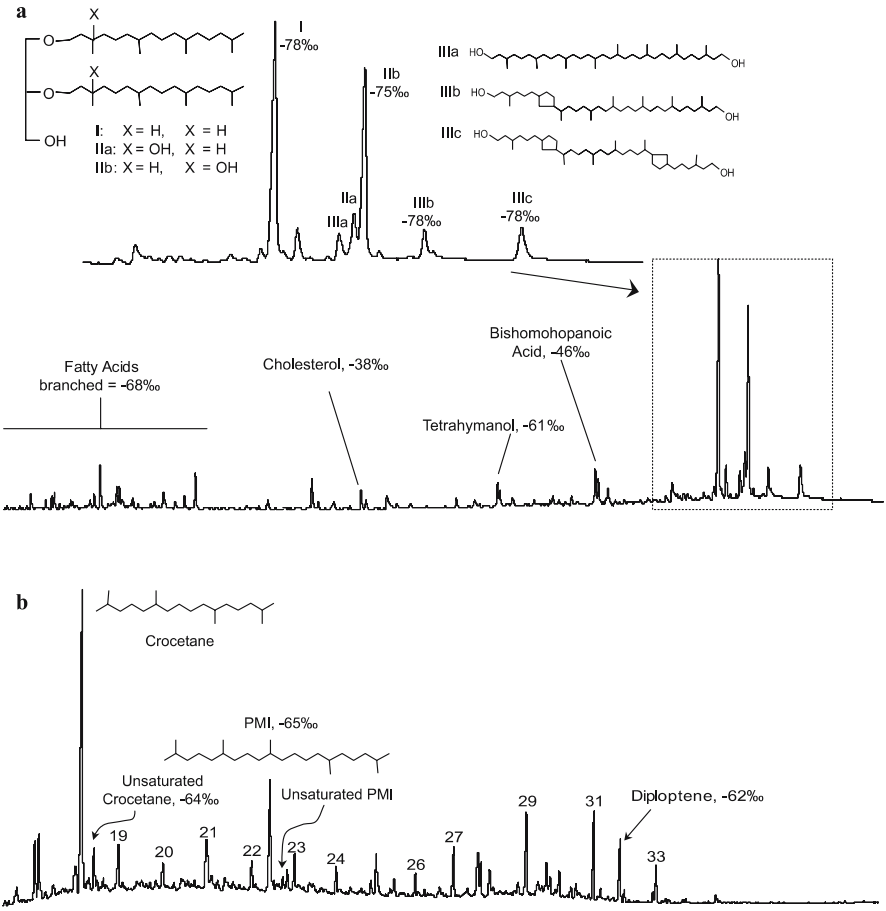

Fig. 11 Partial gas chromatograms showing the relative abundances of archaeal and bacterial biomarkers (and their carbon isotopic compositions) in the polar fraction (**a**) and apolar fraction (**b**) of the total lipid extract of a Napoli Mediterranean mud volcano cold seep. Adapted from [151] and [200]

sites that have been examined are those associated with the Oligocene Lincoln Creek Formation [152, 206], the Miocene Marmorito Limestone [194], the Eocene "Whiskey Creek" deposit [207] and the Jurassic Beauvoisin Formation [208]. These sites contain many of the archaeal (PMI, crocetane, biphytane) and bacterial (hopanes and methyl-branched alcohols, alkanes and alkanoic acids) biomarkers identified in modern cold seep sediments and crusts. Such compounds are typically depleted in ^{13}C (<– 100‰), indicating assimilation of methane and suggesting that the microbial consortia mediating methane oxidation in these ancient sites were similar to those active in modern cold seeps. Thus, determination of biomarker abundances and isotopic compositions in inferred ancient cold seeps can be a powerful additional tool in the identifica-

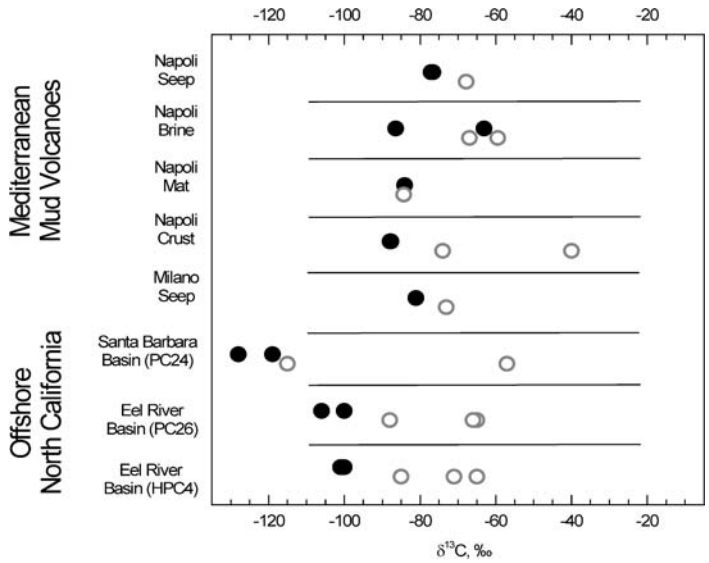

Fig. 12 Plot showing the isotopic offsets between archaeal and bacterial lipid $\delta^{13}C$ values in a range of samples from Mediterranean mud volcano and California margin cold seeps. Adapted from [129] and [199]

tion of AOM and provide a microbiological fingerprint, complementing faunal assemblages in the characterization of such sites.

8 Conclusions and Directions for Future Research

Compound-specific carbon isotopic compositions can help resolve pathways of carbon flow in diverse modern and ancient ecosystems. However, the application of such approaches requires an understanding of: (1) the carbon isotopic composition of likely substrates; (2) the mechanisms of carbon assimilation; (3) carbon isotope effects during assimilation and their sensitivity to environmental conditions; and (4) subsequent isotope effects during lipid biosynthesis. Given these constraints, it is particularly important that assignments of the sources of organic matter used in environmental studies are accurate. Although compound-specific isotope analysis is an important tool in constraining the sources of organic matter being examined, it is vital to continue to identify biomarkers diagnostic for specific organisms and processes. Here we have summarized how alkenone $\delta^{13}C$ values can be used to estimate past pCO_2 levels and how ^{13}C-depleted archaeal and bacterial lipids provide insight into the mechanisms of methane oxidation under anaerobic conditions.

Acknowledgements The authors would like to thank numerous past and present collaborators, including (but certainly not exclusively): Katherine Freeman, Stuart Wakeham, Bob Bidigare, Brian Popp, Jaap Sinninghe Damsté, Stefan Schouten, Giovanni Aloisi, Ioanna Bouloubassi and James Zachos.

References

1. Schidlowski M (1987) Ann Rev Earth Planet Sci 15:47
2. Spiker EC, Hatcher PG, Orem WH (1985) Estuaries 8(2B):A90
3. Hayes JM, Des Marais DJ, Lambert IB, Strauss H, Summons RE (1992) Proterozoic biogeochemistry. In: Schopf JW, Klein C (eds) The Proterozoic biosphere: a multidisciplinary study. Cambridge University Press, Cambridge, p 81–134
4. Ostrom PH, Fry B (1993) Sources and cycling of organic matter within modern and prehistoric food webs. In: Engle MH, Macko SA (eds) Organic geochemistry: principles and applications. Plenum, New York, p 785–798
5. Hayes JM, Freeman KH, Popp BN, Hoham C (1990) Compound-specific isotopic analyses: a novel tool for the reconstruction of ancient biogeochemical processes. In: Durand B, Behar F (eds) Advances in organic geochemistry. Pergamon, Oxford, p 1115–1128
6. Logan GA, Summons RE, Hayes JM (1997) Geochim Cosmochim Acta 61:5391
7. Calder JA, Parker PL (1973) Geochim Cosmochim Acta 37:133
8. Morris I (1980) Paths of carbon assimilation in marine phytoplankton. In: Falkowski P (ed) Primary productivity of the sea. Plenum, New York, p 139–159
9. Degens ET, Guillard RRL, Sackett WM, Hellebust JA (1968) Deep Sea Res 15:1
10. Dean WE, Arthur MA, Claypool GE (1986) Mar Geol 70:119
11. Popp BN, Takigiku R, Hayes JM, Louda JW, Baker EW (1989) Am J Sci 289:436
12. Pagani M, Arthur MA, Freeman KH (1999) Paleoceanography 14:273
13. Freeman KH, Hayes JM, Trendel JM, Albrecht P (1990) Nature 343:254
14. Hayes JM (1993) Mar Geol 1:111
15. Schouten S, Hoefs MJL, Koopmans MP, Bosch H-J, Sinninghe Damsté JS (1998) Org Geochem 29:1305
16. Mariotti A, Germon JC, Hubert P, Kaiser P, Letolle R, Tardieux A, Tardieux P (1981) Plant Soil 62:413
17. Preston T, Owens NJP (1985) Biomed Mass Spectrom 12:510
18. Merritt DA, Hayes JM (1994) Anal Chem 66:2336
19. Meier-Augenstein W (1999) J Chromatogr A 842:351
20. Boon JJ, Rijpstra WIC, de Leeuw JW, Schenck PA (1975) Nature 258:414
21. Grimalt J, Alsaad HT, Douabul AAZ, Albaiges J (1985) Naturwissenschaften 72:35
22. Volkman JK (1986) Org Geochem 9:83
23. Wakeham SG, Farrington JW, Gagosian RB, Lee C, de Baar H, Nigrelli GE, Tripp BW, Smith SO, Frew NM (1980) Nature 286:798
24. Marlowe IT, Brassell SC, Eglinton G, Green JC (1984) Org Geochem 6:135
25. Volkman JK, Eglinton G, Corner EDS, Forsberg TEV (1980) Phytochemistry 19:2619
26. Conte MH, Volkman JK, Eglinton G (1994) Lipid biomarkers of the Haptophyta. In: Green JC, Leadbeater BSC (eds) The Haptophyte algae. Clarendon, Oxford, p 351–377
27. Brassell SC, Eglinton G, Marlowe IT, Pflaumann U, Sarnthein M (1986) Nature 320:129

28. Volkman JK, Barrett SM, Blackburn SI, Mansour MP, Sikes EL, Gelin F (1998) Org Geochem 29:1163
29. Withers NW, Tuttle RC, Goad LJ, Goodwin TW (1979) Phytochem 18:71
30. Robinson N, Eglinton G, Brassell SC, Cranwell PA (1984) Nature 308:439
31. Piretti MV, Pagliuca G, Boni L, Pistocchi R, Diamante M, Gazzotti T (1997) J Phycol 33:61
32. Pancost RD, Freeman KH, Wakeham SG, Robinson CY (1997) Geochim Cosmochim Acta 61:4983
33. Pancost RD, Freeman KH, Wakeham SG (1999) Org Geochem 30:319
34. Eek ME, Whiticar MJ, Bishop JKB, Wong CS (1999) Deep-Sea Res II 46:2863
35. Popp BN, Trull T, Kenig F, Wakeham SG, Rust TM, Tilbrook B, Griffiths FB, Wright SW, Marchant HJ, Bidigare RR, Laws EA (1999) Global Biogeochem Cycles 13:827
36. Schouten S, Van Kaam-Peters HME, Rijpstra WIC, Schoell M, Sinninghe Damsté JS (2000) Am J Sci 300:1
37. Volkman JK, Barrett SM, Dunstan GA (1994) Org Geochem 21:407
38. Rowland SJ, Robson JN (1990) Mar Environ Res 30:191
39. Versteegh GJM, Bosch HJ, de Leeuw JW (1997) Org Geochem 27:1
40. Volkman JK, Jeffrey SW, Nichols PD, Rogers GI, Garland CD (1989) J Exp Mar Biol Ecol 128:219
41. Bell MV, Dick JR, Pond DW (1997) Phytochemistry 45:303
42. Pagani M, Freeman KH, Arthur MA (2000) Geochim Cosmochim Acta 64:37
43. Kuypers MMM, Pancost RD, Sinninghe Damsté JS (1999) Nature 399:342
44. Grice K, Schaeffer P, Schwark L, Maxwell JR (1997) Org Geochem 26:677
45. Eglinton G, Hamilton RJ, Raphael RA, Gonzalez AG (1962) Phytochemistry 1:89
46. Cranwell PA (1981) Org Geochem 3:79
47. Kolattukudy PE (1976) The chemistry and biochemistry of natural waxes. Elsevier, Amsterdam
48. Eglinton G, Hamilton RJ (1967) Science 156:1322
49. Versteegh GJM et al (2004) Geochim Cosmochim Acta 68:411
50. Sarkanen KV, Ludwig CH (1971) Lignins. Wiley, New York
51. Hedges JI, Mann DC (1979) Geochim Cosmochim Acta 43:1809
52. Goñi MA, Yunker MB, Macdonald RW, Eglinton TI (2000) Mar Chem 71:23
53. Huang YS, Freeman KH, Eglinton TI, Street-Perrott FA (1999) Geology 27:471
54. Goñi MA, Teixeira MJ, Perkey DW (2003) Estuar Coast Shelf Sci 57:1023
55. Ourisson G, Rohmer M, Poralla K (1987) Annu Rev Microbiol 41:301
56. Rohmer M, Bisseret P, Neunlist S (1992) In: Moldowan JM, Albrecht P, Philp RP (eds) Biological markers in sediments and petroleum. Prentice-Hall, New Jersey, p 1–17
57. Summons RE, Jahnke LL, Hope JM, Logan GA (1999) Nature 400:554
58. Thiel V, Blumenberg M, Pape T, Seifert R, Michaelis W (2003) Org Geochem 34:81
59. Sinninghe Damsté JS, Rijpstra WIC, Schouten S, Fuerst JA, Jetten MSM, Strous M (2004) Org Geochem 35:561
60. Zundel M, Rohmer M (1985) Eur J Biochem 150:23
61. Gelpi E, Schneider H, Mann J, Oro J (1970) Phytochemistry 9:603
62. Shiea J, Brassell SC, Ward DM (1990) Org Geochem 15:223
63. Liaaen-Jensen S (1978) In: Clayton RK, Sistrom WR (eds) Photosynthetic bacteria. Plenum, New York, p 233–247
64. Koopmans MP, Schouten S, Kohnen MEL, Sinninghe Damsté JS (1996) Geochim Cosmochim Acta 60:4873
65. De Rosa M, Gambacorta A (1988) Prog Lipid Res 27:153
66. Koga Y, Morii H, Akagawa-Matsushita M, Ohga M (1998) Biosci Biotechnol Biochem 62:230

67. Schouten S, Hopmans EC, Pancost RD, Sinninghe Damsté JS (2000) Proc Natl Acad Sci USA 97:14421
68. Hoefs MJL, Schouten S, de Leeuw JW, King LL, Wakeham SG, Sinninghe Damsté JS (1997) Appl Environ Microbiol 63:3090
69. DeLong EF, King LL, Massana R, Cittone H, Murray A, Schleper C, Wakeham SG (1998) Appl Environ Microbiol 64:1133
70. King LL, Pease TK, Wakeham SG (1998) Org Geochem 28:677
71. Pearson A, Eglinton TI (2000) Org Geochem 31:1103
72. Pancost RD, van Geel B, Baas M, Sinninghe Damsté JS (2000) Geology 28:663
73. Holzer G, Oro J, Tornabene TG (1979) J Chromatogr 18:795
74. Risatti JB, Rowland SJ, Yon DA, Maxwell JR (1984) Org Geochem 6:93
75. Brassell SC, Wardroper AMK, Thomson ID, Maxwell JR, Eglinton G (1981) Nature 290:693
76. Schouten S, van der Maarel MJEC, Huber R, Sinninghe Damsté JS (1997) Org Geochem 26:409
77. Elvert M, Suess E, Whiticar MJ (1999) Naturwissenschaften 86:295
78. Bian LQ, Hinrichs KU, Xie TM, Brassell SC, Iversen H, Fossing H, Jorgensen BB, Hayes JM (2001) Geochem Geophys Geosys 2:2000.GC000112
79. Weiss RF (1974) Mar Chem 2:203
80. Mook WG, Bommerson JC, Staberman WH (1974) 22:169
81. Romanek CS, Grossman EL, Morse JW (1992) Geochim Cosmochim Acta 56:419
82. Zhang J, Quay PD, Wilbur DO (1995) Geochim Cosmochim Acta 59:107
83. Halas S, Szaran J, Niezgoda H (1997) Geochim Cosmochim Acta 61:2691
84. Zeebe RE, Wolf-Gladrow D (2001) CO_2 in seawater: equilibrium, kinetics, isotopes. Elsevier, Amsterdam.
85. Hayes JM, Strauss H, Kaufman AJ (1999) Chem Geol 161:103
86. Scholle PA, Arthur MA (1980) Am Assoc Pet Geol Bull 64:67
87. Dickens GR, O'Neil JR, Rea DK, Owen RM (1995) Paleoceanography 10:965
88. Roeske CA, O'Leary MH (1984) Biochemistry 23:6275
89. Raven JA, Johnston AM (1991) Limnol Oceanogr 36:1701
90. Bidigare RR et al (1997) Global Biogeochem Cycles 11:279
91. Popp BN, Laws EA, Bidigare RR, Dore JE, Hanson KL, Wakeham SG (1998) Geochim Cosmochim Acta 62:69
92. Farquhar GD, Richards PA (1984) Aust J Plant Physiol 11:539
93. Sharkey TD, Berry JA (1985) Carbon isotope fractionation of algae as influenced by an inducible CO_2 concentration mechanism. In: Lucas WJ, Berry JA (eds) Inorganic carbon uptake by aquatic photosynthetic organisms. American Society of Plant Physiologists, Rockville, p 389–401
94. Falkowski PG (1991) J Plankton Res 13:21
95. Farquhar GD, O'Leary MH, Berry JA (1982) Aust J Plant Physiol 13:281
96. Laws EA, Bidigare RR, Popp BN (1997) Limnol Oceanogr 42:1552
97. Cassar N, Laws EA, Popp BN, Bidigare RR (2002) Limnol Oceanogr 47:1192
98. Rau GH, Riebesell U, Wolf-Gladrow D (1996) Mar Ecol Prog Ser 133:275
99. Verity PG, Robertson CY, Tronzo CR, Andrews MG, Nelson JR, Sieracki ME (1993) Limnol Oceanogr 37:1434
100. Popp BN, Hanson KL, Dore JE, Bidigare RR, Laws EA, Wakeham SG (1999) Controls on the carbon isotopic composition of phytoplankton: Paleoceanographic perspectives. In: Abrantes F, Mix A (eds) Reconstructing ocean history: a window into the future. Plenum, New York, p 381–398

101. Goericke R, Montoya JP, Fry B (1994) In: Lajtha K, Michener B (eds) Stable isotopes in ecology. Blackwell, Oxford, p 187–221
102. Burns BD, Beardall J (1988) J Exp Mar Biol Ecol 107:75
103. Tortell PD, Reinfelder JR, Morel FMM (1997) Nature 390:243
104. Laws EA, Popp BN, Bidigare RR, Riebesell U, Burkhardt S, Wakeham SG (2001) Geochem Geophys Geosys 2:2000.GC000057
105. Riebesell U, Revill AT, Holdsworth DG, Volkman JK (2000) Geochim Cosmochim Acta 64:4179
106. Francois R, Altabet MA, Goericke R, McCorkle DC, Brunet C, Poisson A (1993) Global Biogeochem Cycles 7:627
107. Friedli H, Lotscher H, Oeschger H, Siegenthaler U, Stauffer B (1986) Nature 324:237
108. Broadmeadow MSJ, Griffiths H (1993) Carbon isotope discrimination and the coupling of CO_2 fluxes within forest canopies. In: Ehleringer JR, Hall AE, Farquhar GD (eds) Stable isotopes and plant carbon–water relations. Academic, San Diego, p 109–129
109. Price GD, McKenzie JE, Pilcher JR, Hoper ST (1997) The Holocene 7:229
110. O'Leary MH (1981) Phytochemistry 20:552
111. Madhavan S, Treichel I, O'Leary MH (1991) Bot Acta 104:292
112. Meinzer FC, Rundel PW, Goldstein G, Sharifi MR (1992) Oecologia 91:305
113. White JWC, Ciais P, Figge RA, Kenny R, Markgraf V (1994) Nature 367:153
114. Sauer M, Maurer S, Matyssek R, Landolt W, Gunthardt-Georg MS, Siegenthaler U (1995) Oecologia 103:397
115. Lockheart MJ, van Bergen PF, Evershed RP (1997) Org Geochem 26:137
116. Libby LM (1972) J Geophys Res 77:4310
117. Libby LM, Pandolfi LJ, Payton PH, Marshall III J, Becker B, Giertz-Sienbenlist V (1976) Nature 261:284
118. Christeller JT, Lang WA, Troughton JH (1976) Plant Physiol 57:580
119. Farmer JG (1979) Nature 279:229
120. Leavitt SW, Long A (1983) Isotope Geosci 1:169
121. Smith BN, Oliver J, McMillan C (1976) Bot Gaz 137:99
122. Troughton JH, Gard KA (1975) Planta 123:185
123. Chikaraishi Y, Naraoka H (2003) Phytochemistry 63:361
124. Marino BD, McElroy MB (1991) Nature 349:127
125. Ehleringer JR, Cerling TE, Helliker BR (1997) Oecologia 112:285
126. Whiticar MJ (1999) Chem Geol 161:291
127. Irwin H, Curtis C, Coleman M (1977) Nature 269:209
128. Elvert M, Suess E, Greinert J, Whiticar MJ (2001) Org Geochem 31:1175
129. Pancost RD, Sinninghe Damsté JS (2003) Chem Geol 195:29
130. Abelson PH, Hoering TC (1961) Proc Natl Acad Sci USA 47:623
131. Deines P (1980) The isotopic composition of reduced organic carbon. In: Fritz P, Fontes JC (eds) Handbook of environmental isotope geochemistry. Elsevier, Amsterdam
132. van der Meer MTJ, Schouten S, van Dongen B, Rijpstra WIC, Fuchs G, Sinninghe Damsté JS, de Leeuw J, Ward DM (2001) J Biol Chem 276:10971
133. van Dongen B, Schouten S, Sinninghe Damsté JS (2001) Rapid Commun Mass Spectrom 15:496
134. Pancost RD, Baas M, van Geel B, Sinninghe Damsté JS (2003) The Holocene 13:921
135. Huang YS, Bol R, Harkness DD, Ineson P, Eglinton G (1996) Org Geochem 24:273
136. Ruby EG, Jannasch HW, Deuser WG (1987) Appl Environ Microbiol 53:1940
137. House CH, Schopf JW, Stetter KO (2003) Org Geochem 34:345

138. Sirevåg R, Buchanan BB, Berry JA, Throughton JH (1977) Arch Microbiol 112:35
139. Quandt I, Gottshalk G, Ziegler H, Stichler W (1977) FEMS Microbiol Lett 1:125
140. Holo H, Sirevåg R (1986) Arch Microbiol 145:173
141. Strauß G, Fuchs G (1993) Eur J Biochem 215:633
142. Menendez C, Bauer Z, Huber H, Gad'on N, Stetter KO, Fuchs G (1999) J Bacteriol 181:1088
143. Preuß A, Schauder R, Fuchs G, Stichler W (1989) Z Naturforsch C 44:397
144. Van der Meer MTJ, Schouten S, Rijpstra WIC, Fuchs G, Sinninghe Damsté JS (2001) FEMS Microbiol Lett 196:67
145. Pearson A, McNichol AP, Benitez-Nelson BC, Hayes JM, Eglinton TI (2001) Geochim Cosmochim Acta 65:3123
146. Kuypers MMM, Blokker P, Erbacher J, Kinkel H, Pancost RD, Schouten S, Sinninghe Damsté JS (2001) Science 293:92
147. Summons RE, Franzmann PD, Nichols PD (1998) Org Geochem 28:465
148. Schouten S, Rijpstra WIC, Kok M, Hopmans EC, Summons RE, Volkman JK, Sinninghe Damsté JS (2001) Geochim Cosmochim Acta 65:1629
149. Jahnke LL, Summons RE, Hope JM, Des Marais DJ (1999) Geochim Cosmochim Acta 63:79
150. Hinrichs K-U, Hayes JM, Sylva SP, Brewer PG, DeLong EF (1999) Nature 398:802
151. Pancost RD, Sinninghe Damsté JS, de Lint S, van der Maarel MJEC, Gottschal JC (2000) The MEDINAUT Shipboard Scientific Party. Appl Environ Microbiol 66:1126
152. Thiel V, Peckmann J, Richnow HH, Luth U, Reitner J, Michaelis W (2001) Mar Chem 73:97
153. Teece MA, Fogel ML, Dollhopf ME, Nealson KH (1999) Org Geochem 30:1571
154. Zhang CL, Li Y, Ye E, Fong J, Peacock AD, Blunt E, Fang J, Lovley D, White DC (2003) Chem Geol 195:17
155. Monson KD, Hayes JM (1982) Geochim Cosmochim Acta 46:139
156. DeNiro MJ, Epstein S (1977) Science 197:261
157. Blair N, Leu A, NuAmerican Society of Plant Physiologists, Rockvillenoz E, Olsen J, Kwong E, Des Marais D (1985) Appl Environ Microbiol 50:996
158. Rohmer M, Sutter B, Sahm H (1989) J Chem Soc Chem Commun 19:1471
159. Rohmer M, Knani M, Simonin P, Sutter B, Sahm H (1993) Biochem J 295:517
160. Horbach S, Sahm H, Welle R (1993) FEMS Microbiol Lett 111:135
161. Rohmer M, Seeman M, Horbach S, Bringer-Meyer S, Sahm H (1996) J Am Chem Soc 118:2564
162. Lichtenthaler HK, Rohmer M, Schwender J (1997) Physiol Plant 101:643
163. Disch A, Schwender J, Muller C, Lichtenthaler HK, Rohmer M (1998) Biochem J 333:381
164. Schouten S, Breteler W, Blokker P, Schogt N, Rijpstra WIC, Grice K, Baas M, Sinninghe Damsté JS (1998) Geochim Cosmochim Acta 62:1397
165. Pancost RD, Freeman KH, Wakeham SG (1999) Org Geochem 30:319
166. Popp BN, Trull T, Kenig F, Wakeham SG, Rust TM, Tilbrook B, Griffiths FB, Wright SW, Marchant HJ, Bidigare RR, Laws EA (1999) Global Biogeochem Cycles 13:827
167. Collister JW, Rieley G, Stern B, Eglinton G, Fry B (1994) Org Geochem 21:619
168. Goñi MA, Ruttenberg KC, Eglinton TI (1997) Nature 389:275
169. Summons RE, Jahnke LL, Roksandik Z (1994) Geochim Cosmochim Acta 58:2853
170. van der Meer MTJ, Schouten S, Sinninghe Damsté JS (1998) Org Geochem 28:527
171. Sakata S, Hayes JM, McTaggart AR, Evans RA, Leckrone KJ, Togasaki RK (1997) Geochim Cosmochim Acta 61:5379

172. Bidigare RR et al (1999) Global Biogeochem Cycles 13:251
173. Rau GH, Takahashi T, Des Marais DJ, Repeta DJ, Martin JH (1992) Geochim Cosmochim Acta 56:1413
174. Jasper JP, Mix AC, Prahl FG, Hayes JM (1994) Paleoceanography 6:781
175. Jasper JP, Hayes JM (1990) Nature 347:462
176. Andersen N, Müller PJ, Kirst G, Schneider RR (1999) The $\delta^{13}C$ signal in $C_{37:2}$ alkenones as a proxy for reconstructing Late Quaternary pCO_2 in surface waters from the South Atlantic. In: Fischer G, Wefer G (eds) Proxies in paleoceanography: examples from the South Atlantic. Springer, Berlin Heidelberg New York, p 469–488
177. Pagani M, Freeman KH, Arthur MA (1999) Science 285:876
178. Nimer NA, Dixon GK, Merrett MJ (1992) New Phytol 120:153
179. Nimer NA, Guan Q, Merrett MJ (1994) New Phytol 126:601
180. Nimer NA, Merrett MJ (1996) New Phytol 133:383
181. Rost B, Zondervan I, Riebesell U (2002) Limnol Oceanogr 47:120
182. Pagani M, Freeman KH, Ohkouchi N, Caldeira K (2002) Paleoceanography 17:1069
183. Ohkouchi N, Kawamura K, Kawahata H, Okada H (1999) Global Biogeochem Cycles 13:695
184. Tsubota H, Ishizaka J, Nishimura A, Watanabe YW (1999) J Oceanogr 55:645
185. Blair NE, Aller RC (1995) Geochim Cosmochim Acta 59:3707
186. Borowski WS, Paull CK, Ussler W III (1996) Geology 24:655
187. Burns SJ (1998) Geochim Cosmochim Acta 62:797
188. Iverson N, Jørgensen BB (1985) Limnol Oceanogr 30:944
189. Reeburgh WS (1980) Earth Planet Sci Lett 46:345
190. Reeburgh WS (1996) Soft spots in the global methane budget. In: Lidstrom ME, Tabita FR (eds) Microbial growth on C_1 compounds. Kluwer, Dordrecht, p 334–342
191. Boetius A, Ravenschlag K, Schubert CJ, Rickert D, Widdel F, Gieseke A, Amann R, Jørgensen BB, Witte U, Pfannkuche (2000) Nature 407:623
192. Zhang CLL, Li YL, Wall JD, Larsen L, Sassen R, Huang YS, Wang Y, Peacock A, White DC, Horita J, Cole DR (2002) Geology 30:239
193. Zhang CL, Pancost RD, Sassen R, Qian Y, Macko SA (2003) Org Geochem 34:827
194. Thiel V, Peckmann J, Seifert R, Wehrung P, Reitner J, Michaelis W (1999) Geochim Cosmochim Acta 63:3959
195. Schouten S, Wakeham SG, Sinninghe Damsté JS (2001) Org Geochem 32:1277
196. Wakeham SG, Lewis CM, Hopmans EC, Schouten S, Sinninghe Damsté JS (2003) Geochim Cosmochim Acta 67:1359
197. Teske A, Hinrichs K-U, Edgcomb V, Gomez AD, Kysela D, Sylva SP, Sogin ML, Jannasch HW (2002) Appl Environ Microbiol 68:1994
198. Orphan VJ, House CH, Hinrichs KU, McKeegan KD, DeLong EF (2001) Science 293:484
199. Hinrichs K-U, Summons RE, Orphan V, Sylva SP, Hayes JM (2000) Org Geochem 31:1685
200. Pancost RD, Hopmans EC, Sinninghe Damsté JS (2001) The MEDINAUT Shipboard Scientific Party. Geochim Cosmochim Acta 65:1611
201. Pancost RD, Bouloubassi I, Aloisi G, Sinninghe Damsté JS (2001) The MEDINAUT Shipboard Scientific Party. Org Geochem 32:695
202. Werne JP, Baas M, Sinninghe Damsté JS (2002) Limnol Oceanogr 47:1694
203. Elvert M, Boetius A, Knittel K, Jorgensen BB (2003) Geomicrobiol J 20:403
204. Valentine DL, Reeburgh WS (2000) Environ Microbiol 25:477
205. Hoehler TM, Alperin MJ, Albert DB, Martens CS (1994) Geochim Cosmochim Acta 43:739

206. Peckmann J, Thiel V, Michaelis W, Clari P, Gaillard C, Martire L, Reitner J (1999) Int J Earth Sci 88:60
207. Goedert JL, Thiel V, Schmale O, Rau WW, Michaelis W, Peckmann J (2003) Facies 48:223
208. Peckmann J, Thiel V, Michaelis W, Clari P, Gaillard C, Martire L, Reitner J (1999) Int J Earth Sci 88:60
209. Boschker HTS, Nold SC, Wellsbury P, Bos D, de Graaf W, Pel R, Parkes RJ, Cappenberg TE (1998) Nature 392:801
210. Bull ID, Parekh NR, Hall GH, Ineson P, Evershed RP (2000) Nature 405:175
211. Laws EA, Popp BN, Bidigare RR, Kennicutt MC, Macko SA (1995) Geochim Cosmochim Acta 59:1131
212. Laws EA, Landry MR, Barber RT, Campbell L, Dickson ML, Marra J (2000) Deep-Sea Res II 47:1339
213. Prahl FG, Muehlhausen LA, Zahnle DL (1988) Geochim Cosmochim Acta 52:2303